isvr Institute of Sound and Vibration Research

Further Study of Indirect Force Determination and Transfer Path Analysis Using Numerical Simulations for a Flat Plate

A.N. Thite and D.J. Thompson

ISVR Technical Memorandum 854

October 2000

University of Southampton

SCIENTIFIC PUBLICATIONS BY THE ISVR

Technical Reports are published to promote timely dissemination of research results by ISVR personnel. This medium permits more detailed presentation than is usually acceptable for scientific journals. Responsibility for both the content and any opinions expressed rests entirely with the author(s).

Technical Memoranda are produced to enable the early or preliminary release of information by ISVR personnel where such release is deemed to the appropriate. Information contained in these memoranda may be incomplete, or form part of a continuing programme; this should be borne in mind when using or quoting from these documents.

Contract Reports are produced to record the results of scientific work carried out for sponsors, under contract. The ISVR treats these reports as confidential to sponsors and does not make them available for general circulation. Individual sponsors may, however, authorize subsequent release of the material.

UNIVERSITY OF SOUTHAMPTON

INSTITUTE OF SOUND AND VIBRATION RESEARCH

DYNAMICS GROUP

Further Study of Indirect Force Determination and Transfer Path Analysis Using Numerical Simulations for a Flat Plate

by

A.N. Thite and D.J. Thompson

ISVR Technical Memorandum No. 854

October 2000

Contents

1. Introduction

In experimental transfer path analysis (TPA) [1-4], effective diagnosis of the noise problems depends on reliable force identification. The force identification is, however, prone to errors. In particular, where forces are determined indirectly by inversion of frequency response function (eg. accelerance) matrices, errors are introduced by the ill-conditioning of the accelerance matrix at certain frequencies. If the accelerance matrix is badly conditioned, small errors in the measurement of accelerances and operational accelerations are magnified by the matrix operations and result in erroneous force estimates. Since the force identification determines the contribution of different forces to the sound pressure at receiver locations, these errors are propagated.

An earlier study [5] considered a rectangular simply supported plate as a test structure. Numerical simulations were performed for 4 or 6 simultaneous coherent forces and various strategies of reconstructing forces from measured responses in the presence of noise were investigated. To improve the force identification, in [5] singular value rejection was implemented based on the norm of the accelerance error matrix. In addition resampling of the accelerance matrix was investigated and found to improve the force and response estimates. The importance of considering the phase information when averaging over a number of samples was also emphasized in that study.

The forces used in [5] were coherent and had zero phase difference. It is interesting to investigate the sensitivity of force identification if a fixed non-zero phase difference is incorporated. This formulation is explained in chapter 2 and results are given. The added complication of incoherent or partially coherent forces is not introduced at this stage, although it can be dealt with using procedures given in [2].

The conclusions in [5] may be sensitive to the particular choice of noise model used for corrupting the responses and accelerances to simulate the 'measurements'. In [5] a Gaussian noise of rather small amplitude was assumed. It is important to determine the sensitivity of the conclusions to the noise amplitude, and to different formulations such as a proportional noise model. In chapter 3 the effect of increased noise amplitude on the force identification and response prediction is investigated. A proportional noise model is incorporated in chapter 4, and results analysed.

An improved force identication was achieved in ref [5] by the rejection of singular values based on the threshold established by the norm of the accelerance error matrix. It was observed that the results from this strategy were dependent on the band of error used i.e +/- one or three standard deviation. In general the use of +/- one standard deviation resulted in better predictions. However, the improvement was not so significant at frequencies in the vicinity of anti-resonance. This could be due to the fact that the errors in accelerance measurement and operational response measurement are not related. This in turn may lead to inconsistency in the reconstruction of forces. It might, however, be possible to improve the force identification and hence the response at the receiver location if singular values are rejected based on the error in the operational response measurments. This strategy is formulated and analysed in chapter 5.

The H_1 estimator is a most commonly used frequency response function estimator in structural analysis and was used in [5]. Since it is not a good estimator near the resonance frequencies it might be possible to improve the force identification at resonance by constructing the accelerance matrix based on the H_2 estimator instead of H_1. This, however, may be dis-advantageous in the regions of anti-resonance. Other estimators also exist which attempt to combine the advantages of H_2 and H_1. These are explained in

chapter 6 along with the discussion on the force identification for respecive frequency response estimators.

It is observed that for good understanding and effective implementation of TPA, it is important to formulate the propagation of errors in each step. The error propagation is modelled in [6] for both random and bias errors. These models are explained in Appendix and error propagation results are discussed in chapter 7.

2. Effect of fixed non-zero phase in coherent forces

2.1 Introduction

The forces used in [5] to study the different strategies were coherent and had zero phase difference. The conclusions drawn there might have been influenced by the nature of these forces. Hence, it is interesting to investigate the sensitivity of force identification if a phase difference other than zero is incorporated.

In this study, a non-zero phase at each frequency is incorporated into the forces. The phase at each frequency is generated using uniformly distributed random numbers. It can be written as below

Force=**constant x** $e^{j2\pi N}$, where N is a vector containing uniformly distributed random numbers varying between 0 and 1, different for each frequency

Note : The phase difference once generated by this process is retained and used for all trials in this section.

The forces generated by the above process are then used in generating the acceleration responses on the rectangular flat plate at several locations, along with an appropriate noise model, as in [5]. The accelerances from all forcing locations to all response locations are also simulated as in [5]. The typical 1/3 octave noise spectra, as added to the inputs and outputs of accelerance measurements, are shown in Figures 1a and 1b. The same noise model is used for both the accelerances and operational responses. A typical transfer mobility for one of the force positions to one of the response positions is shown in Figure 2. The influence of measurement noise can be seen at high frequencies and is very clear from the fall in coherence. Figure 3 shows operational velocity response for

one of the response positions. This can be compared with the noise spectra given in Figure 1b.

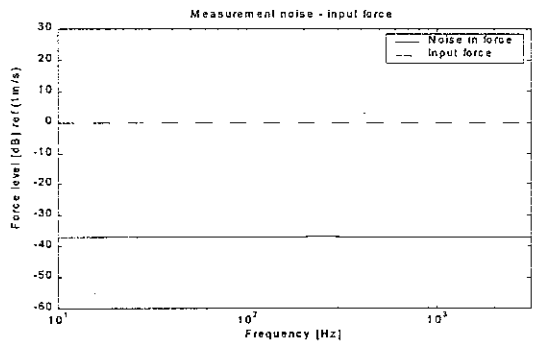

Figure 1a. 1/3 octave band noise in the measurement of force during accelerance measurement

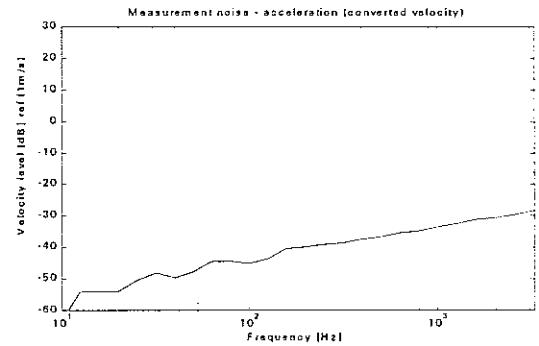

Figure 1b. 1/3 octave band noise in the measurement of acceleration converted to velocity

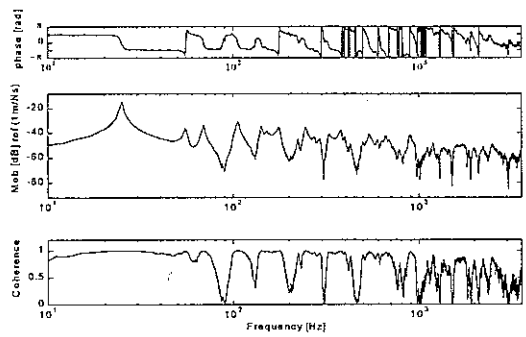

Figure 2. Transfer mobility from excitation point 1 to response point 1

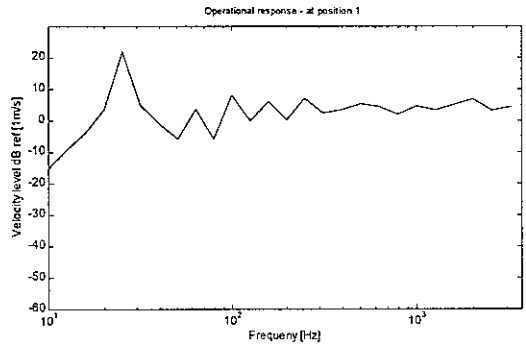

Figure 3. Velocity at position 1 for combined action of first four forces as in [5]

2.2 Force reconstruction

The forces are reconstructed by the inversion of the accelerance matrix and using operational accelerations. As in [5], the following are compared

1. Use of full rank matrix (all singular values used)

2. Singular value rejection based on the norm of the accelerance error matrix

3. Resampling of accelerances

Figures 4a-b show the singular values of the accelerance matrix and the reconstructed forces for 4 forces and 4 responses (n_r=n_e=4) when all singular values are used. The force reconstruction is quite poor in the low frequency region where the condition numbers of the accelerance matrix are high. However the force reconstruction remains similar to the case where the forces are in phase ([5] see Figure 14). The reconstructed sum of forces is also shown in the figure. Figures 5a-b show the singular values used at each frequency and the forces reconstructed when singular values are rejected based on the threshold established by the norm of the accelerance error matrix constructed from +/- 3 standard deviations in the estimation of accelerance. These results are comparable with those obtained when using forces that are in phase ([5] see Figure 10). The same is the case with resampling (Figures 6a-b) and singular value rejection based on the error band of +/- one standard deviation (Figures 7a-b).

The force reconstruction for the cases n_r=6, n_e=4 is shown in Figures 8-10, while Figures 11-13 show results for n_r=6, n_e=6. All these results are in agreement with what is obtained when forces are in phase (compare with [5]).

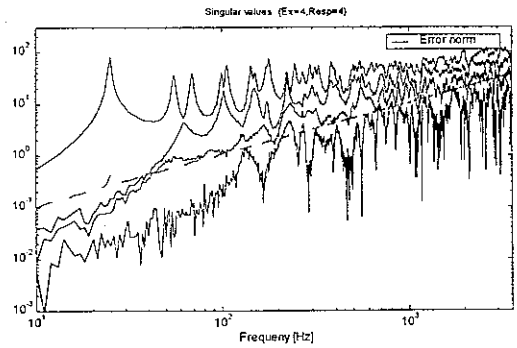

Figure 4a. Singular values along with error norm of accelerance matrix for 4 sources and 4 responses

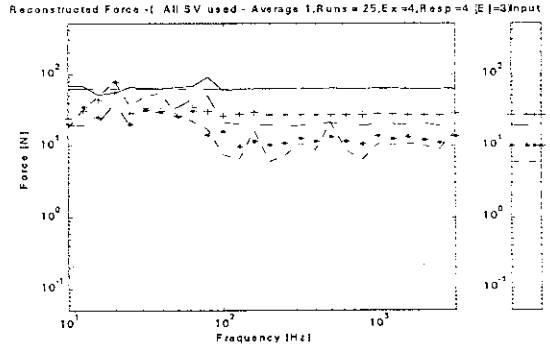

Figure 4b. 1/3 octave band reconstructed forces for 4 sources and 4 responses with all singular values used

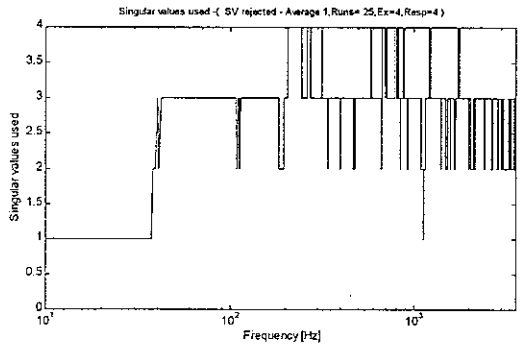

Figure 5a. Number of Singular values used at each frequency for 4 sources and 4 responses. Singular values rejected based on the error band of +/- 3 std. deviation in accelerance estimation.

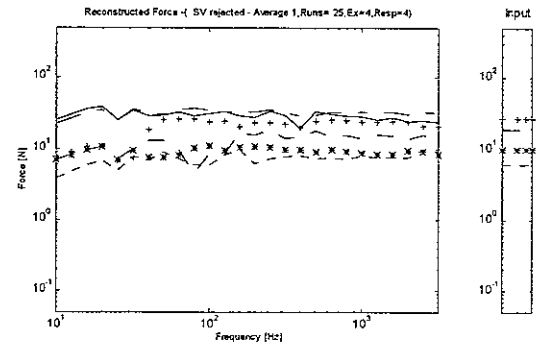

Figure 5b. 1/3 octave band reconstructed forces for 4 sources and 4 responses. Singular values rejected based on the error band of +/- 3 std. deviation in accelerance estimation.

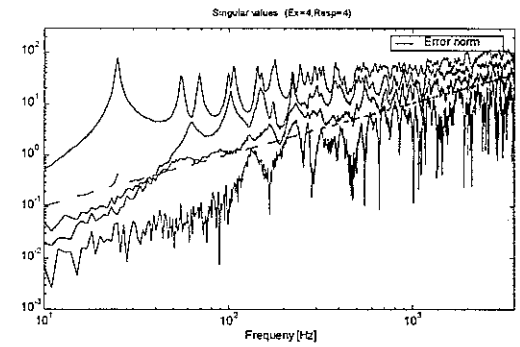

Figure 6a. Singular values along with error norm of accelerance matrix for 4 sources and 4 responses

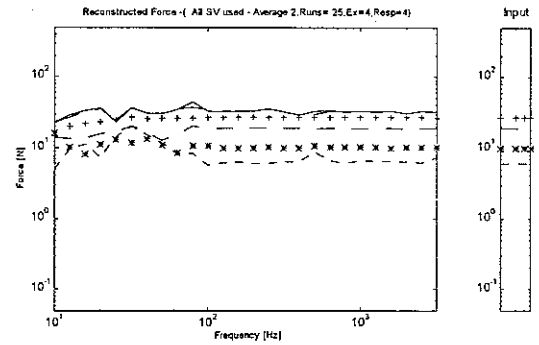

Figure 6b. 1/3 octave band reconstructed forces for 4 sources and 4 responses with all singular values used with resampling

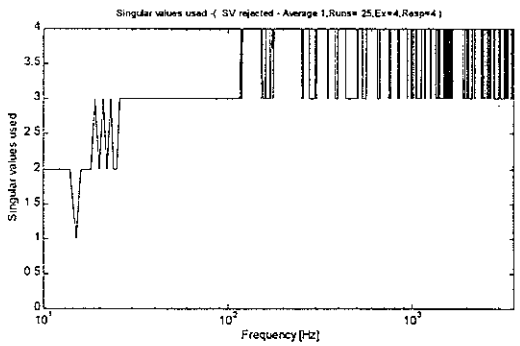

Figure 7a. Number of Singular values used at each frequency for 4 sources and 4 responses. Singular values rejected based on the error band of +/- one std. deviation in accelerance estimation.

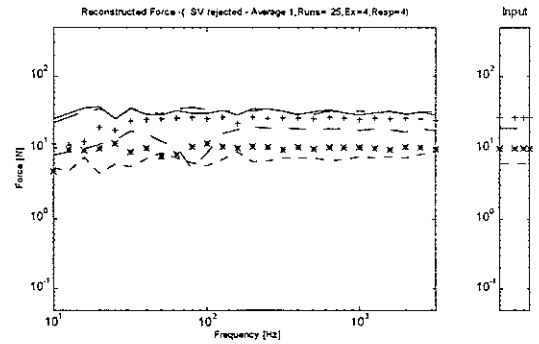

Figure 7b. 1/3 octave band reconstructed forces for 4 sources and 4 responses. Singular values rejected based on the error band of +/- one std. deviation in accelerance estimation.

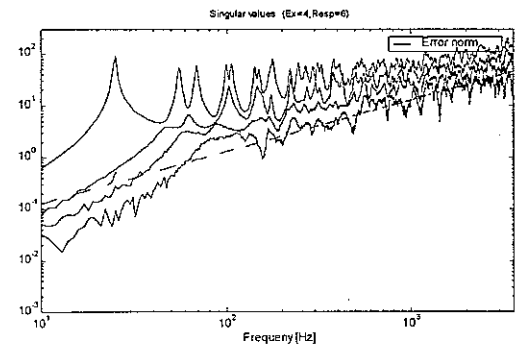

Figure 8a. Singular values along with error norm of accelerance matrix for 4 sources and 6 responses

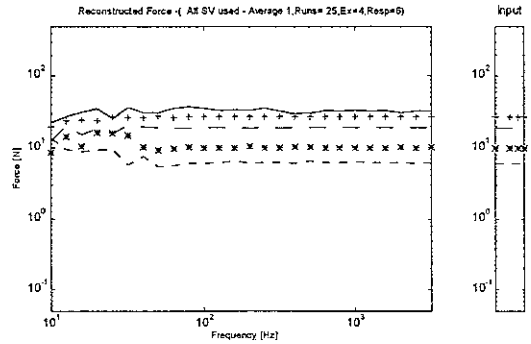

Figure 8b. 1/3 octave band reconstructed forces for 4 sources and 6 responses with all singular values used

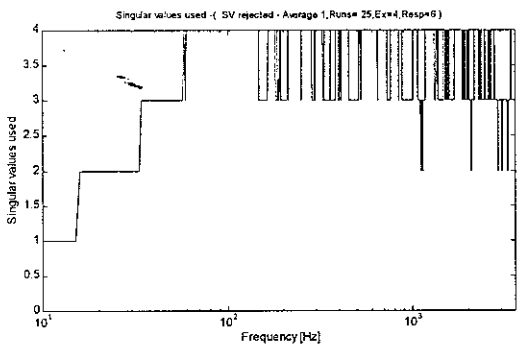

Figure 9a. Number of Singular values used at each frequency for 4 sources and 6 responses. Singular values rejected based on the error band of +/- 3 std. deviation in accelerance estimation.

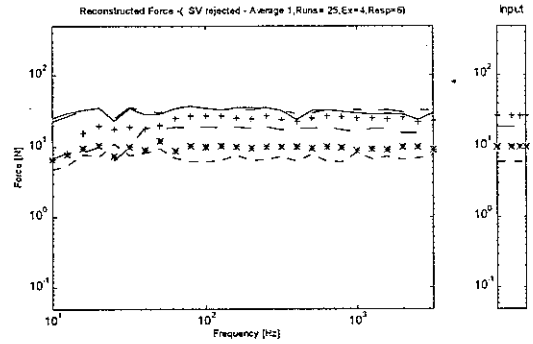

Figure 9b. 1/3 octave band reconstructed forces for 4 sources and 6 responses. Singular values rejected based on the error band of +/- 3 std. deviation in accelerance estimation

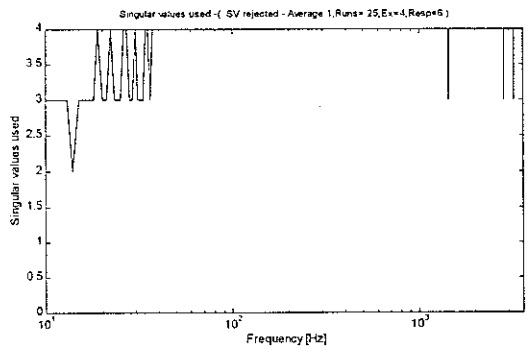

Figure 10a. Number of Singular values used at each frequency for 4 sources and 6 responses. Singular values rejected based on the error band of +/- one std. deviation in accelerance estimation

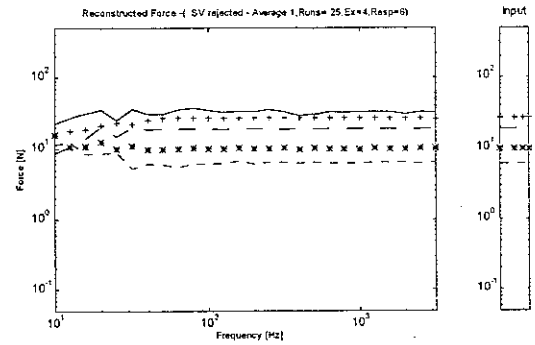

Figure 10b. 1/3 octave band reconstructed forces for 4 sources and 6 responses. Singular values rejected based on the error band of +/- one std. deviation in accelerance estimation

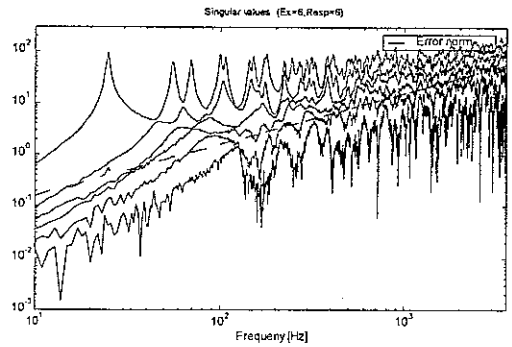

Figure 11a. Singular values along with error norm of accelerance matrix for 6 sources and 6 responses

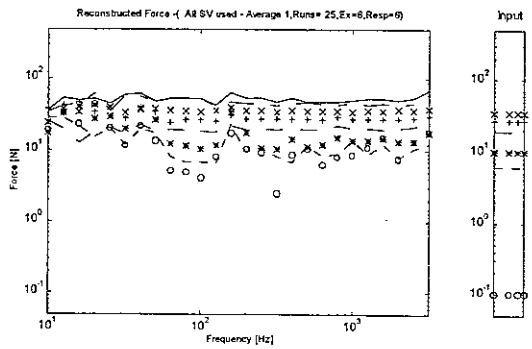

Figure 11b. 1/3 octave band reconstructed forces for 6 sources and 6 responses with all singular values used

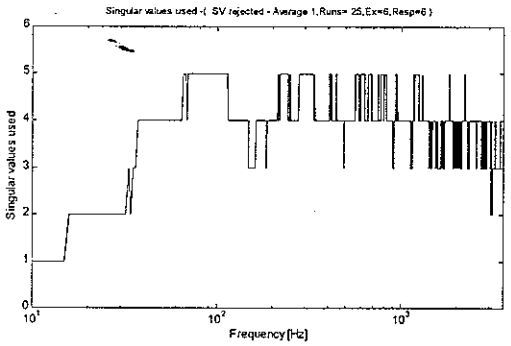

Figure 12a. Number of Singular values used at each frequency for 6 sources and 6 responses. Singular values rejected based on the error band of +/- 3 std. deviation in accelerance estimation

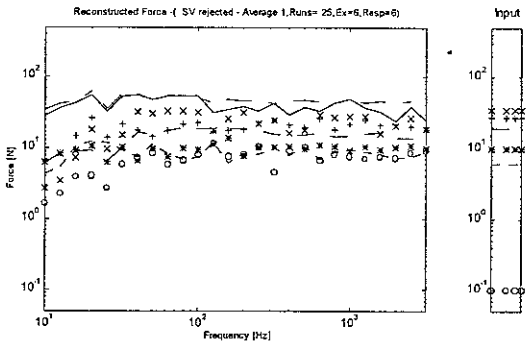

Figure 12b. 1/3 octave band reconstructed forces for 6 sources and 6 responses. Singular values rejected based on the error band of +/- 3 std. deviation in accelerance estimation

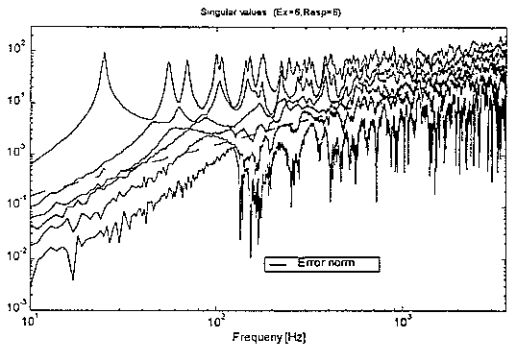

Figure 13a. Singular values along with error norm of accelerance matrix for 6 sources and 6 responses

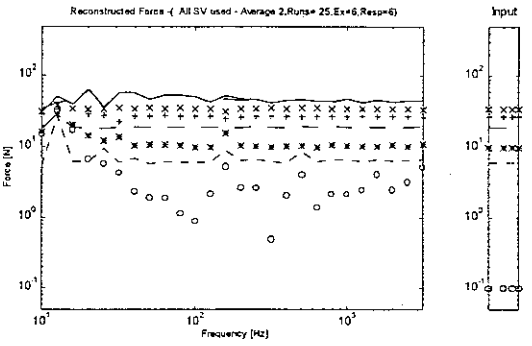

Figure 13b. 1/3 octave band reconstructed forces for 6 sources and 6 responses with all singular values used and resampling

2.3 Velocity at the receiver location

Figures 14a-d show the 1/3 octave band velocity response at the receiver location for $n_r=n_e=4$. At low frequencies, the predictions seem to depend on the reliablity of estimating the sum of the forces as concluded in [5].

The predictions using singular value rejection based on the error norm calculated from +/- one standard deviation are more reliable than either those with all singular values used or using singular value rejection based on the error norm with +/- 3 standard deviation in the estimation of accelerance (compare Figure 14d with 14a-b). However the velocity prediction in the region of 60-90Hz does not improve for the above case. Figure 14c shows the response when accelerances are resampled. The prediction is accurate in this case compared to when single accelerances are used or singular values are rejected. These conclusions are comparable to those derived when the forces are in phase [5].

Figures 15a-c show the velocity responses for $n_r=6$, $n_e=4$, while Figures 16a-c show results for $n_r=6$, $n_e=6$. All these results are consistent with what was obtained when the forces are in phase (compare with [5]).

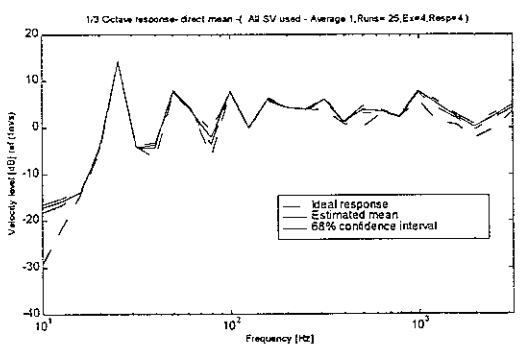

Figure 14a. 1/3 octave band velocity response for 4 sources and 4 responses with all singular values used

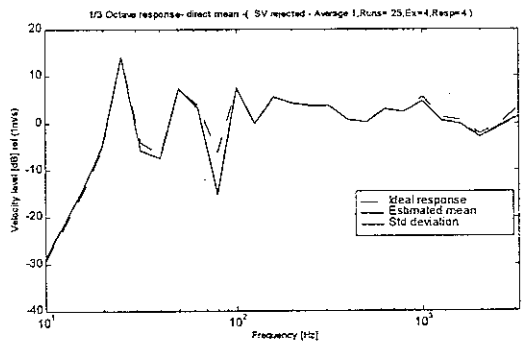

Figure 14b. 1/3 octave band velocity response for 4 sources and 4 responses with singular value rejection based on error band of +/- 3 std. deviation in accelerance

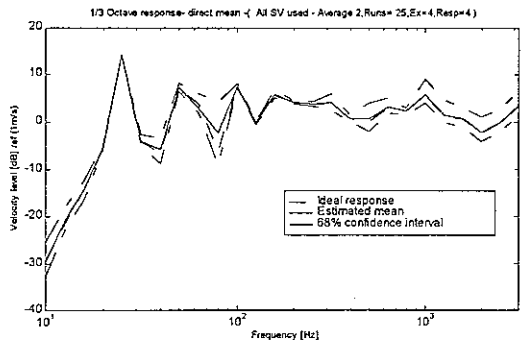

Figure 14c. 1/3 octave band velocity response for 4 sources and 4 responses with all singular values used and resampling

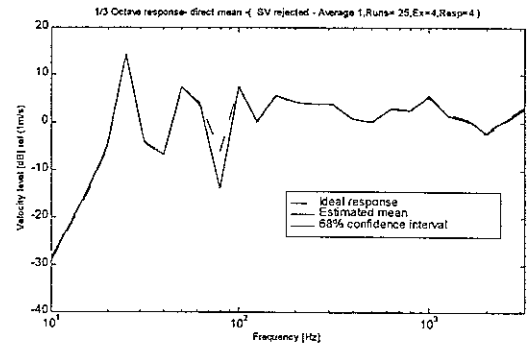

Figure 14d. 1/3 octave band velocity response for 4 sources and 4 responses with singular value rejection based on error band of +/- one std. deviation in accelerance

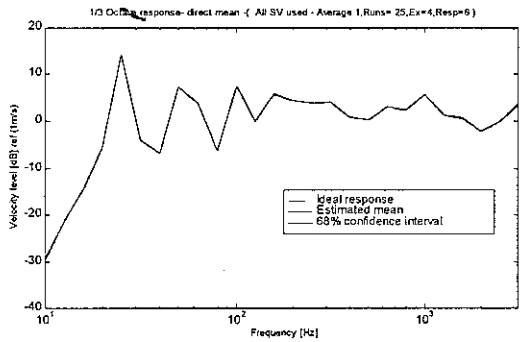

Figure 15a. 1/3 octave band velocity response for 4 sources and 6 responses with all singular values used

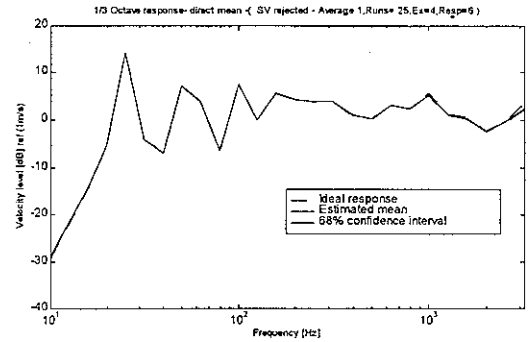

Figure 15b. 1/3 octave band velocity response for 4 sources and 6 responses with singular value rejection based on error band of +/- 3 std. deviation in accelerance

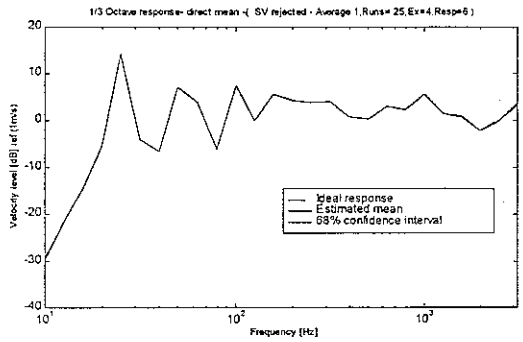

Figure 15c. 1/3 octave band velocity response for 4 sources and 6 responses with singular value rejection based on error band of +/- one std. deviation in accelerance

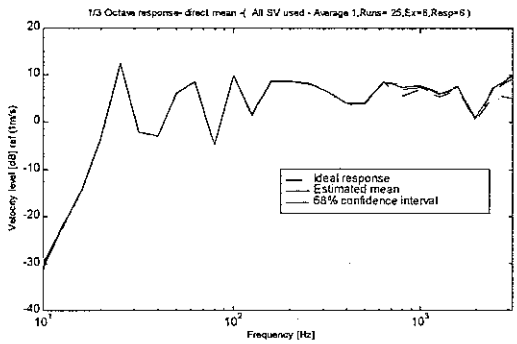

Figure 16a. 1/3 octave band velocity response for 6 sources and 6 responses with all singular values used

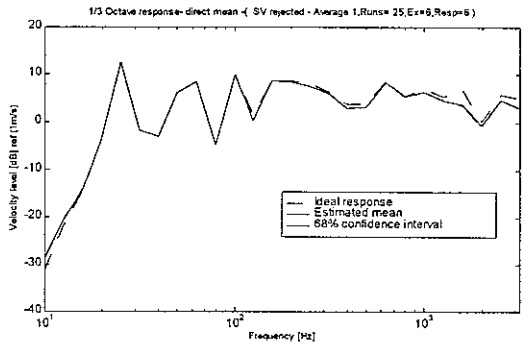

Figure 16b. 1/3 octave band velocity response for 6 sources and 6 responses with singular value rejection based on error band of +/- 3 std. deviation in accelerance

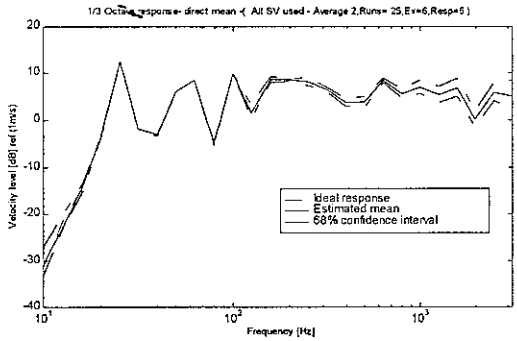

Figure 16c. 1/3 octave band velocity response for 6 sources and 6 responses with all singular values used and resampling

2.4 Conclusions

The characteristics of the reconstructed forces, and hence of the 1/3 octave band response at the receiver location, do not change when the forces used have a definite phase difference other than zero.

3. Experiments with considerable noise

In [5], while simulating the conditions to represent the experiments, Gaussian noise models with either constant amplitude or amplitude proportional to frequency were used. The amplitude at each frequency, however, was significantly lower than the operational acceleration at any response location. Similar noise was added in both operational response and accelerance measurements. The conclusions in [5] might be sensitive to the amplitude of the corrupting noise. Hence, it is important to investiagte the sensitivity of the conclusions to the noise amplitude. In this chapter the influence of high amplitude noise on the force reconstruction and the response prediction is studied. Two sets of predictions are considered: in the first the noise amplitude increases with frequency, in the second the amplitude is constant with frequency.

3.1 Noise proportional to frequency

The measurement noise used in corrupting the acceleration response is shown in Figure 17a. This can be compared with one of the operational accelerances given in Figure 17b. At higher frequencies, above 1000 Hz, the noise amplitude is similar to the acceleration amplitude. The noise in the acceleration used in this case is Gaussian with amplitude proportional to the frequency. When converted converted velocity this gives a flat which increases at 10 dB/decade in a 1/3 octave spectrum. Figure 18 shows the noise amplitude in the input signal. Based on these noise models, accelerances are estimated and one of the accelerances is shown in Figure 19. From the coherence plot it can be seen that the accelerance is particularly noisy for frequencies above 1000 Hz.

Using the same procedure as in [5], the forces are reconstructed and velocity response at the receiver location is predicted. The results are discussed below.

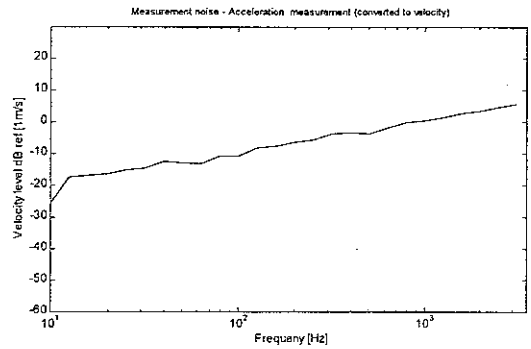

Figure 17a. 1/3 octave band noise in the measurement of acceleration converted to velocity -noise proportional to frequency

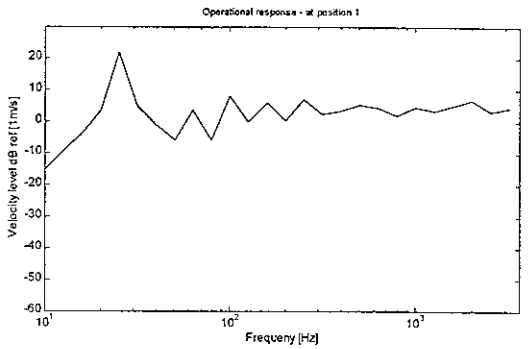

Figure 17b. Velocity at position 1 for combined action of first four forces as in [5] -noise proportional to frequency

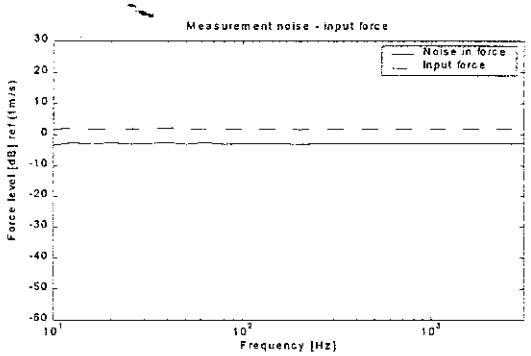

Figure 18. 1/3 octave band noise in the measurement of force during accelerance measurement

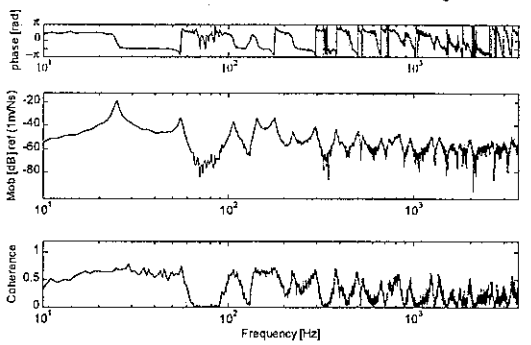

Figure 19. Transfer mobility from excitation point 1 to response point 1-noise proportional to frequency

3.2 Force reconstruction

Figures 20a-b show the singular values of the accelerance matrix and the reconstructed forces for $n_r=n_e=4$ when all singular values are used. The force reconstruction is quite poor throughout the frequency range used for study. In this case it does not matter whether the accelerance matrix has a higher condition number or not. Figures 21a-b show the singular values used at each frequency and the forces reconstructed when singular values are rejected based on the threshold established by the norm of accelerance error matrix constructed from +/- 3 standard deviations in the estimation of accelerance. The sum of forces is always under-estimated as a large proportion of the singular values are

rejected at each frequency. The force reconstruction improves remarkably when singular values are rejected based on the error band of +/- one standard deviation in accelerance estimation (Figures 23a-b), even though the measurement noise in the accelerations is high. Figures 22a-b show the results when resampling of the accelerance matrix is applied [5]. The force reconstruction has large errors but it is better than the cases where all singular values are used (Figure 20) or singular value rejection is based on the error band of +/- 3 standard deviation (Figure 21). However, it is quite inferior to that when singular values are rejected based on the error band of +/- one standard deviation (Figure 23).

The force reconstructions for the cases n_r=6, n_e=4 are shown in Figures 24-26. The force reconstruction improves considerably for all singular values used (compare Figures 24 and 20) and for singular value rejection based +/- one standard deviation in accelerance estimation (compare Figures 26 and 23). However, the force reconstruction is always inferior with large noise amplitude compared to the rather small amplitude used in [5].

The reconstructed forces for n_r=6, n_e=6 are shown in Figures 27-29. The above conclusions remain valid for these cases as well.

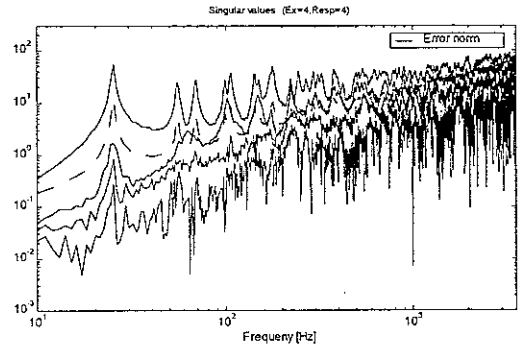

Figure 20a. Singular values along with error norm of accelerance matrix for 4 sources and 4 responses - noise proportional to frequency

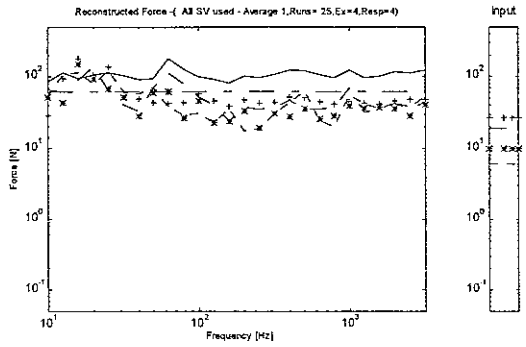

Figure 20b. 1/3 octave band reconstructed forces for 4 sources and 4 responses with all singular values used- noise proportional to frequency

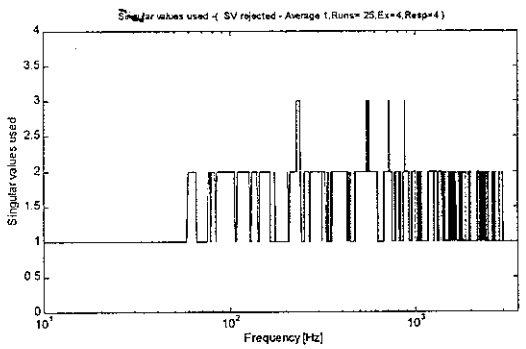

Figure 21a. Number of Singular values used at each frequency for 4 sources and 4 responses. Singular values rejected based on the error band of +/- 3 std. deviation in accelerance estimation - noise proportional to frequency

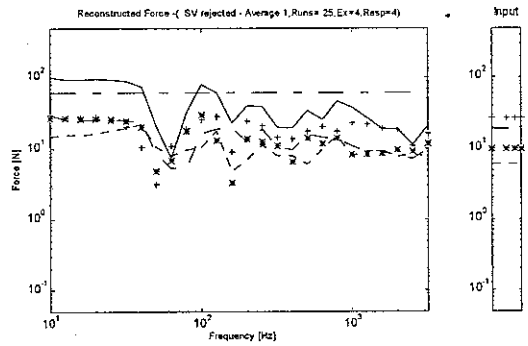

Figure 21b. 1/3 octave band reconstructed forces for 4 sources and 4 responses. Singular values rejected based on the error band of +/- 3 std. deviation in accelerance estimation - noise proportional to frequency

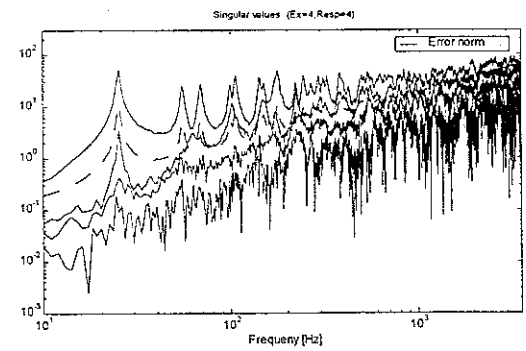

Figure 22a. Singular values along with error norm of accelerance matrix for 4 sources and 4 responses - noise proportional to frequency

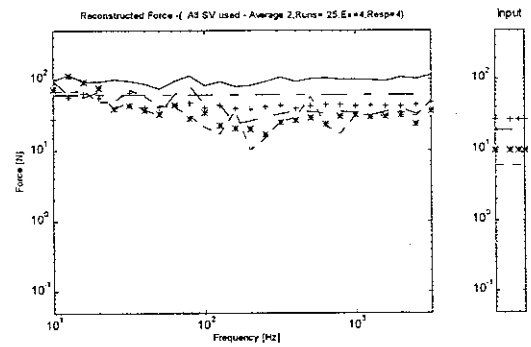

Figure 22b. 1/3 octave band reconstructed forces for 4 sources and 4 responses with all singular values used and resampling - noise proportional to frequency

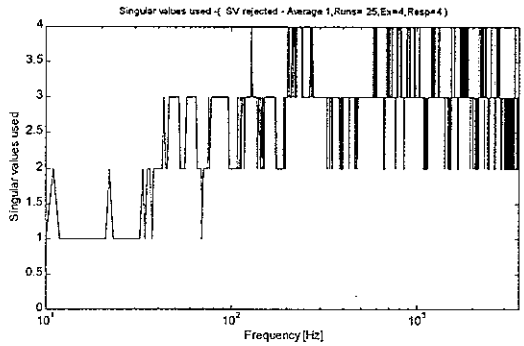

Figure 23a. Number of Singular values used at each frequency for 4 sources and 4 responses. Singular values rejected based on the error band of +/- one std. deviation in accelerance estimation - noise proportional to frequency

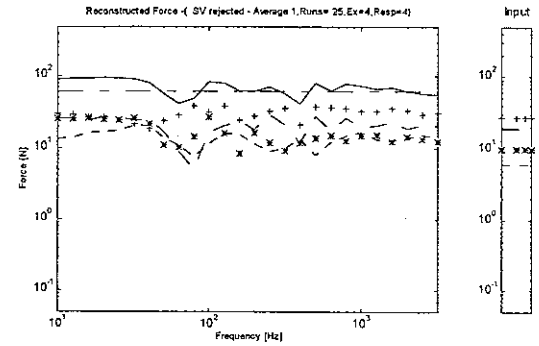

Figure 23b. 1/3 octave band reconstructed forces for 4 sources and 4 responses. Singular values rejected based on the error band of +/- one std. deviation in accelerance estimation - noise proportional to frequency

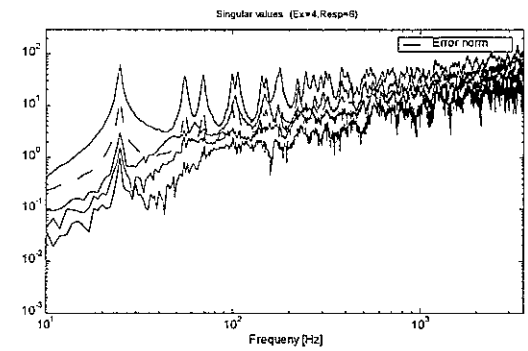

Figure 24a. Singular values along with error norm of accelerance matrix for 4 sources and 6 responses - noise proportional to frequency

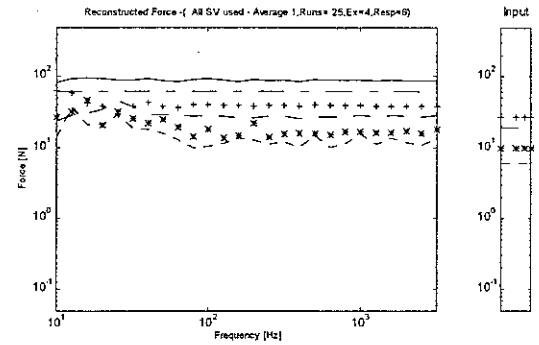

Figure 24b. 1/3 octave band reconstructed forces for 4 sources and 6 responses with all singular values used - noise proportional to frequency

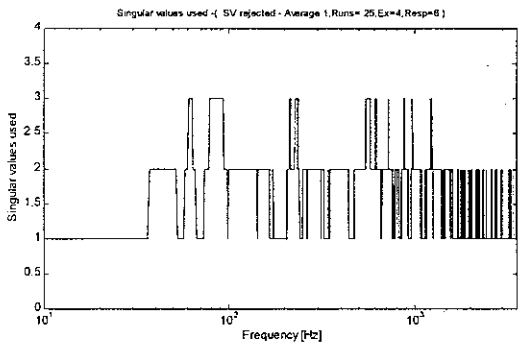

Figure 25a. Number of Singular values used at each frequency for 4 sources and 6 responses. Singular values rejected based on the error band of +/- 3 std. deviation in accelerance estimation - noise proportional to frequency

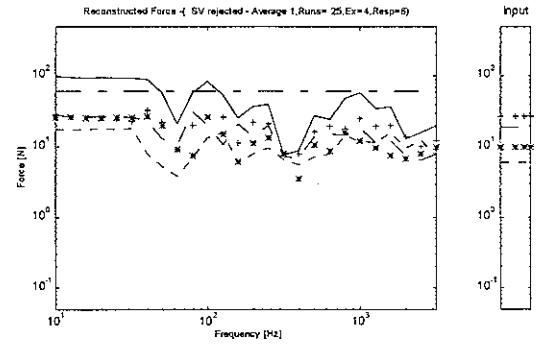

Figure 25b. 1/3 octave band reconstructed forces for 4 sources and 6 responses. Singular values rejected based on the error band of +/- 3 std. deviation in accelerance estimation - noise proportional to frequency

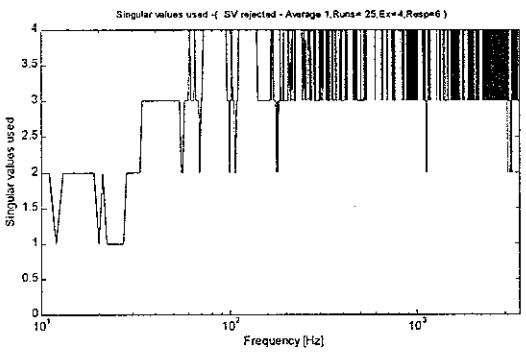

Figure 26a. Number of Singular values used at each frequency for 4 sources and 6 responses. Singular values rejected based on the error band of +/- one std. deviation in accelerance estimation - noise proportional to frequency

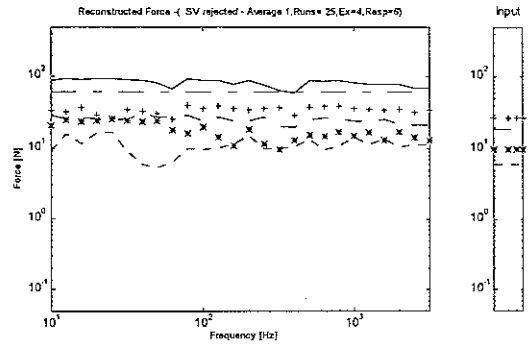

Figure 26b. 1/3 octave band reconstructed forces for 4 sources and 6 responses. Singular values rejected based on the error band of +/- one std. deviation in accelerance estimation - noise proportional to frequency

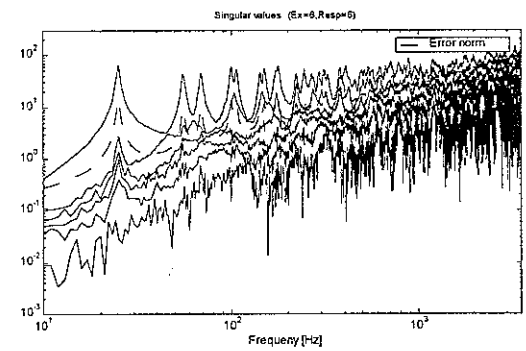

Figure 27a. Singular values along with error norm of accelerance matrix for 6 sources and 6 responses - noise proportional to frequency

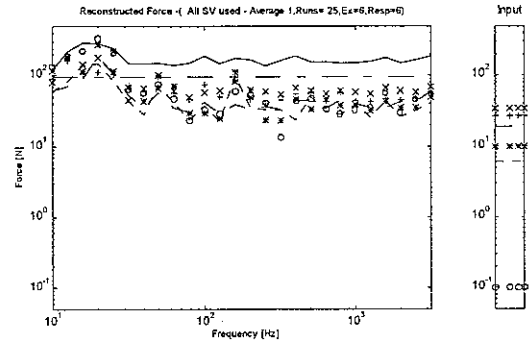

Figure 27b. 1/3 octave band reconstructed forces for 6 sources and 6 responses with all singular values used - noise proportional to frequency

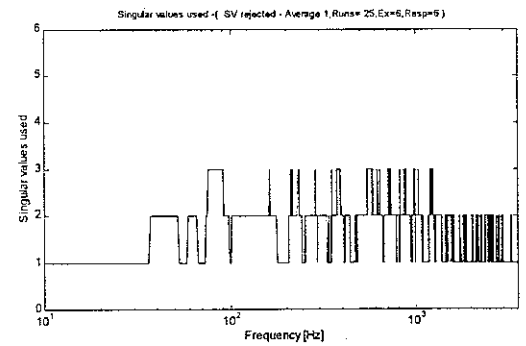

Figure 28a. Number of Singular values used at each frequency for 6 sources and 6 responses. Singular values rejected based on the error band of +/- 3 std. deviation in accelerance estimation - noise proportional to frequency

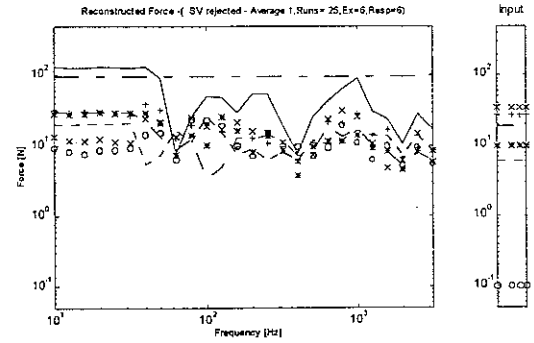

Figure 28b. 1/3 octave band reconstructed forces for 6 sources and 6 responses. Singular values rejected based on the error band of +/- 3 std. deviation in accelerance estimation - noise proportional to frequency

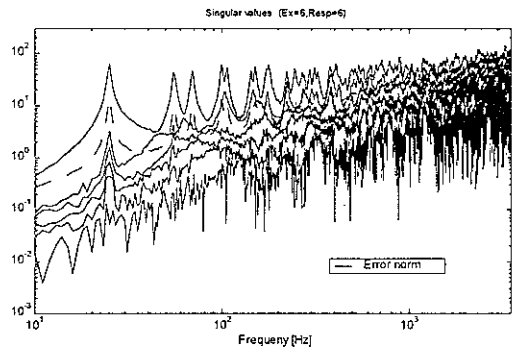

Figure 29a. Singular values along with error norm of accelerance matrix for 6 sources and 6 responses - noise proportional to frequency

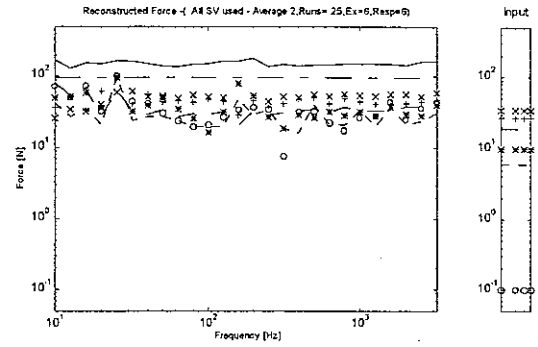

Figure 29b. 1/3 octave band reconstructed forces for 6 sources and 6 responses with all singular values used and resampling - noise proportional to frequency

3.3 Velocity at the receiver location

Figures 30a-d show the 1/3 octave band velocity response at the receiver location for $n_r=n_e=4$. The velocity response predicted at higher frequencies with all singular values used is quite poor whether or not phase information is used in the averaging process as shown in Figures 30a-b. The response is accurate only in the vicinity of the first mode of the rectangular plate.

The results when singular values are rejected based on the error band of +/- 3 standard deviations are shown in Figures 30c-d. Compared to the cases when all singular values are used (Figures 30a-b) the prediction at the receiver location has improved considerably. However the velocity prediction in the high frequency range is lower than the actual result. This is because the sum of the forces is under-estimated across the whole frequency range (Figure 21b). The velocity response improves further when singular values are rejected based on the error band of +/- one standard deviation in the estimation of accelerance as shown in the Figures 30g-h. The averaging with phase

information included results in better prediction (compare Figure 30g and 30h). The resampling strategy results in predictions with large errors compared to those for singular value rejection (Figures 30e-f and 30g-h). The resampling strategy is observed to be very sensitive to the amplitude of the corrupting noise. The velocity prediction improves significantly, however, for averaging with phase information when a large number of averages is taken (in this study 25 averages are taken, improvement is observed with 200 averages). Thus it is seen that the singular value rejection strategy is least sensitive to the noise amplitude, although the results differ considerably based on the size of the error band used in constructing the error matrix.

The velocity prediction improves for an overdetermined system (n_r=6, n_e=4), as shown in Figures 31a-f (compare with Figures 30). Figures 32a-f show results for n_r=6, n_e=6. In both cases the low frequency prediction improves compared to n_r=4, n_e=4. The singular value rejection method, again, gives the best prediction (Figure 32c-d).

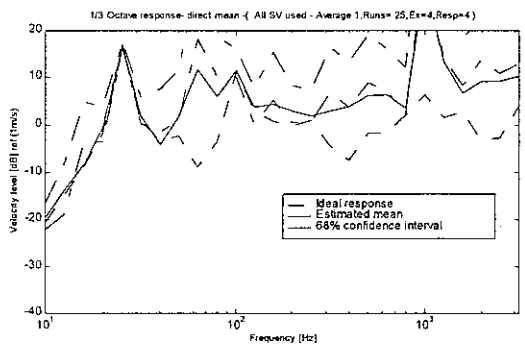

Figure 30a. 1/3 octave band velocity response for 4 sources and 4 responses with all singular values used (with phase information) - noise proportional to frequency

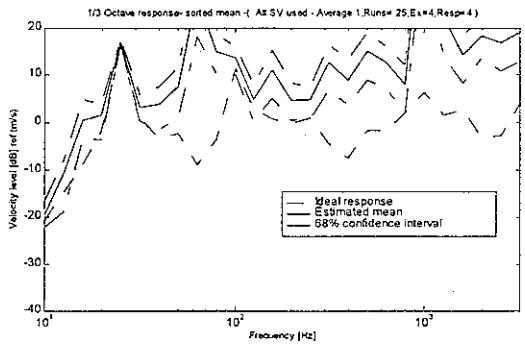

Figure 30b. 1/3 octave band velocity response for 4 sources and 4 responses with all singular values used (no phase information)- noise proportional to frequency

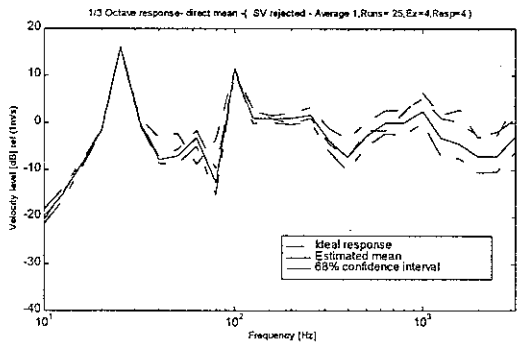

Figure 30c. 1/3 octave band velocity response for 4 sources and 4 responses with singular value rejection based on error band of +/- 3 std. deviation in accelerance (with phase information) - noise proportional to frequency

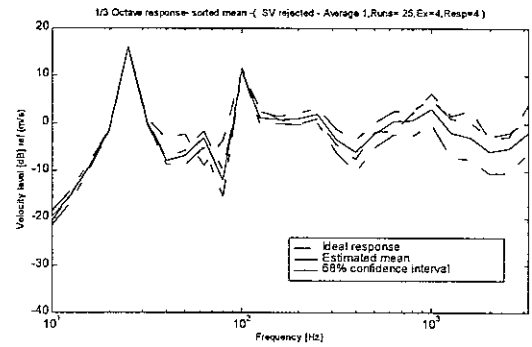

Figure 30d. 1/3 octave band velocity response for 4 sources and 4 responses with singular value rejection based on error band of +/- one std. deviation in accelerance (no phase information) - noise proportional to frequency

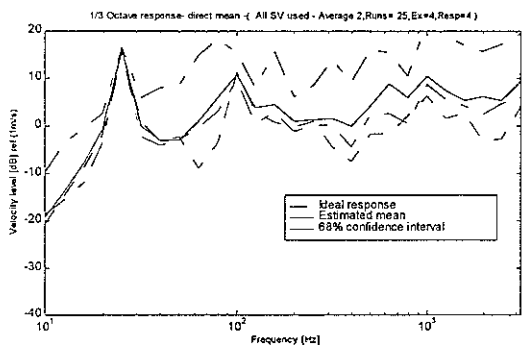

Figure 30e. 1/3 octave band velocity response for 4 sources and 4 responses with all singular values used and resampling (with phase information) - noise proportional to frequency

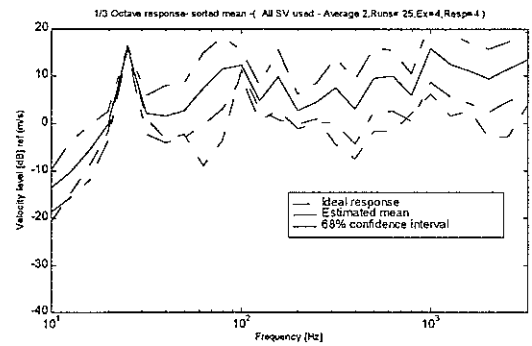

Figure 30f. 1/3 octave band velocity response for 4 sources and 4 responses with all singular values used and resampling (no phase information) - noise proportional to frequency

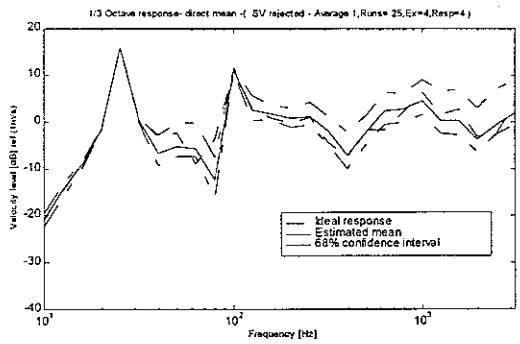

Figure 30g. 1/3 octave band velocity response for 4 sources and 4 responses with singular value rejection based on error band of +/- one std. deviation in accelerance (with phase information) - noise proportional to frequency

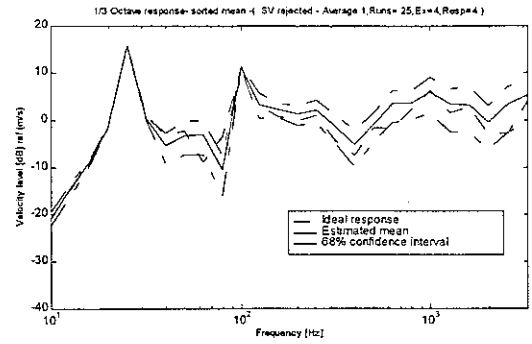

Figure 30h. 1/3 octave band velocity response for 4 sources and 4 responses with singular value rejection based on error band of +/- one std. deviation in accelerance (no phase information) - noise proportional to frequency

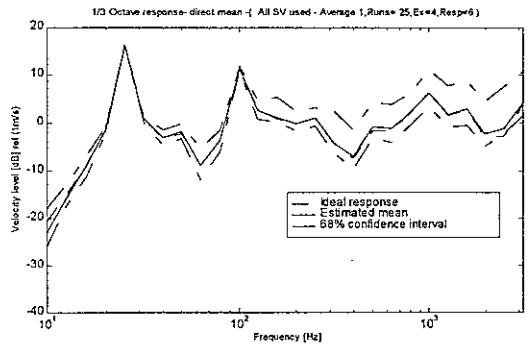

Figure 31a. 1/3 octave band velocity response for 4 sources and 6 responses with all singular values (with phase information) - noise proportional to frequency

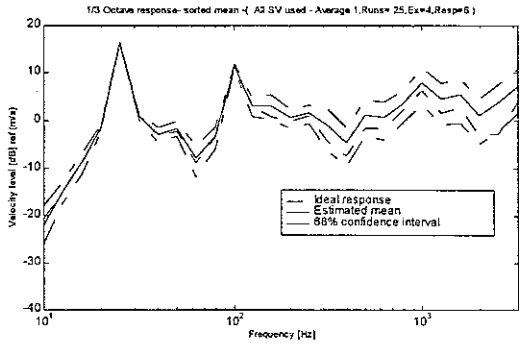

Figure 31b. 1/3 octave band velocity response for 4 sources and 6 responses with all singular values (no phase information) - noise proportional to frequency

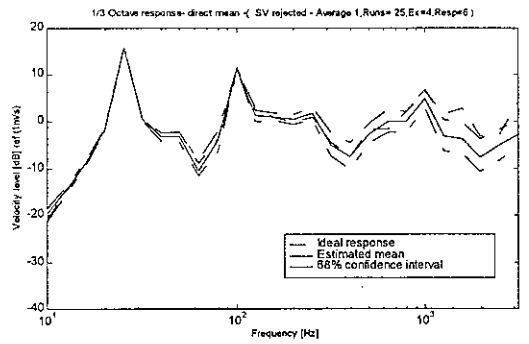

Figure 31c. 1/3 octave band velocity response for 4 sources and 6 responses with singular value rejection based on error band of +/- 3 std. deviation in accelerance (with phase information) - noise proportional to frequency

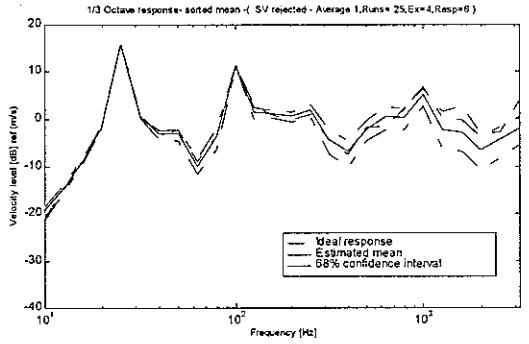

Figure 31d. 1/3 octave band velocity response for 4 sources and 6 responses with singular value rejection based on error band of +/- 3 std. deviation in accelerance (no phase information) - noise proportional to frequency

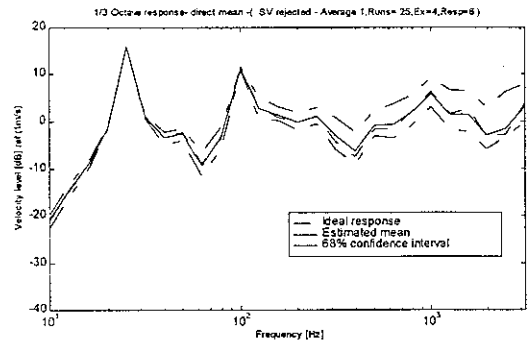

Figure 31e. 1/3 octave band velocity response for 4 sources and 6 responses with singular value rejection based on error band of +/- one std. deviation in accelerance (with phase information) - noise proportional to frequency

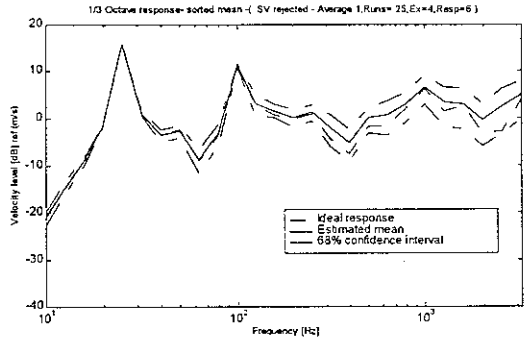

Figure 31f. 1/3 octave band velocity response for 4 sources and 6 responses with singular value rejection based on error band of +/- one std. deviation in accelerance (no phase information) - noise proportional to frequency

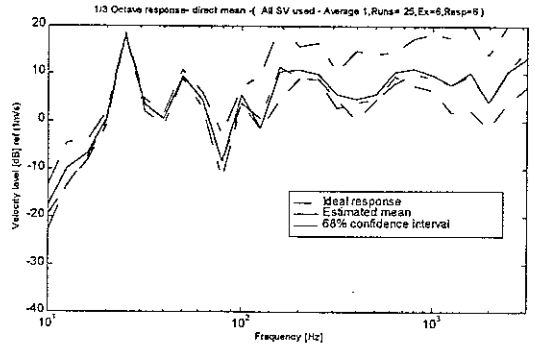

Figure 32a. 1/3 octave band velocity response for 6 sources and 6 responses with all singular values (with phase information) - noise proportional to frequency

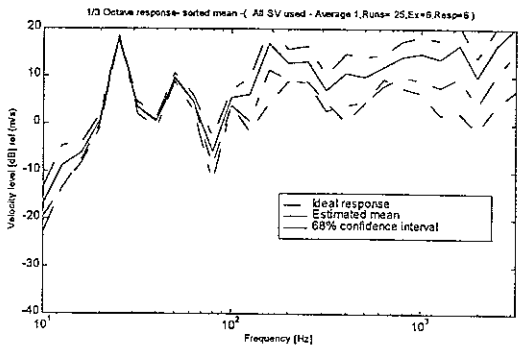

Figure 32b. 1/3 octave band velocity response for 6 sources and 6 responses with all singular values (no phase information) - noise proportional to frequency

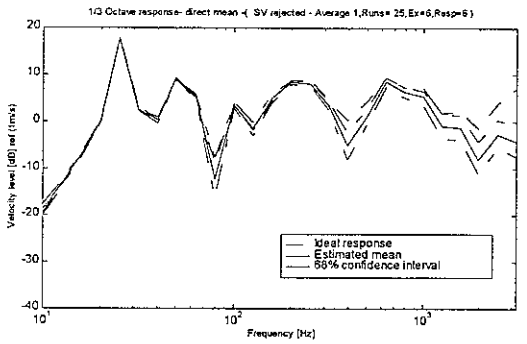

Figure 32c. 1/3 octave band velocity response for 6 sources and 6 responses with singular value rejection based on error band of +/- 3 std. deviation in accelerance (with phase information) - noise proportional to frequency

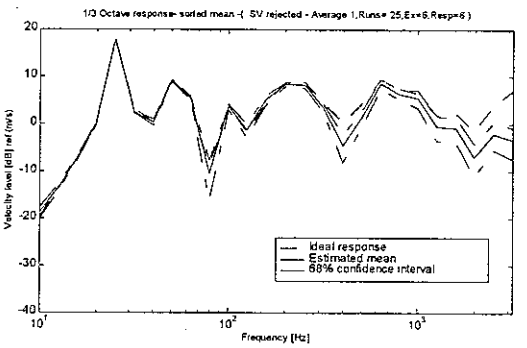

Figure 32d. 1/3 octave band velocity response for 6 sources and 6 responses with singular value rejection based on error band of +/- 3 std. deviation in accelerance (no phase information) - noise proportional to frequency

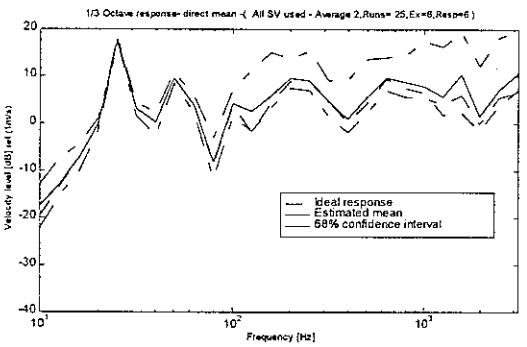

Figure 32e. 1/3 octave band velocity response for 6 sources and 6 responses with all singular values and resampling (with phase information) - noise proportional to frequency

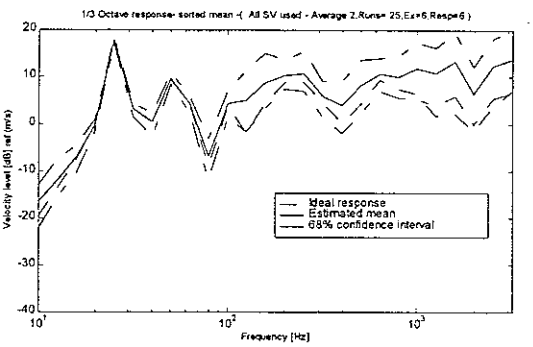

Figure 32f. 1/3 octave band velocity response for 6 sources and 6 responses with all singular values and resampling (no phase information) - noise proportional to frequency

3.4 Noise constant with frequency

The measurement noise used in corrupting the acceleration response for this case is a Gaussian constant level spectrum (it therefore falls with frequency when converted to velocity). It has very high amplitude at low frequency compared to the operational acceleration (compare Figures 33a and 33b). Figure 34 shows the noise amplitude in the input signal. Based on these noise models, the accelerances are estimated and one of these is shown in Figure 35. From the coherence plot it can be seen that the accelerance is particularly noisy in the low frequency region.

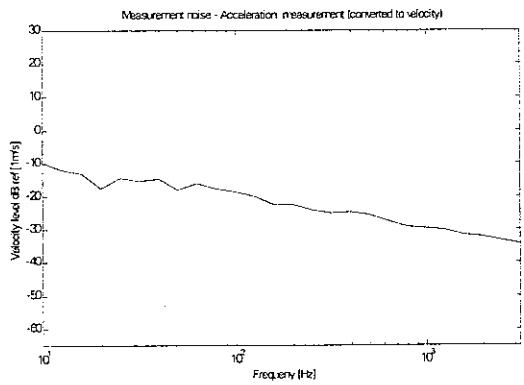

Figure 33a. 1/3 octave band noise in the measurement of acceleration converted to velocity -noise proportional to frequency

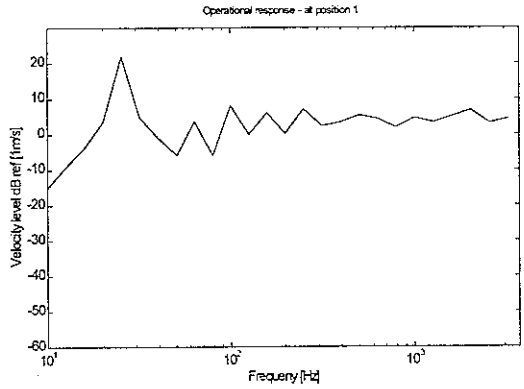

Figure 33b. Velocity at position 1 for combined action of first four forces as in [5] -noise proportional to frequency

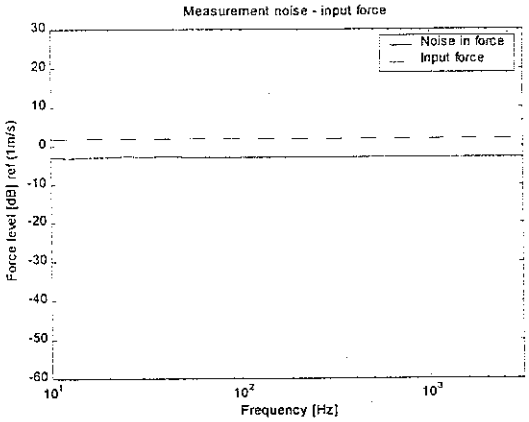

Figure 34. 1/3 octave band noise in the measurement of force during accelerance measurement

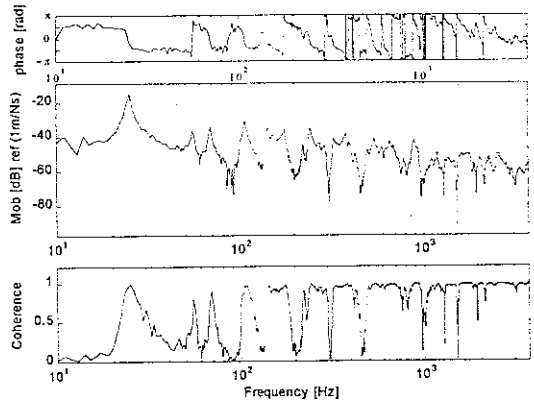

Figure 35. Transfer mobility from excitation point 1 to response point 1-noise proportional to frequency

Using the same procedure as in [5], the forces are reconstructed and velocity response at the receiver location is predicted. The results are discussed below.

3.5 Force reconstruction

Figures 36a-b show the singular values of the accelerance matrix and the reconstructed forces for $n_r=n_e=4$ when all singular values are used. The force reconstruction is quite poor in the low frequency range up to 200 Hz. It improves, however, at higher frequencies. Figures 37a-b show the singular values used at each frequency and the forces reconstructed when singular values are rejected based on the threshold established by the norm of accelerance error matrix constructed from the band of +/- 3 standard deviation in the estimation of accelerance. The forces are under-estimated in the low frequency range as a large proportion of singular values are rejected at each of the frequencies in this region. When singular values are rejected based on the error band of +/- one standard deviation in accelerance estimation (Figures 39a-b), the force reconstruction improves to some extent across the entire frequency range. However, the force reconstruction remains poor in the frequency range from 40 to 100 Hz. Figures 38a-b show the results for resampling. The force reconstruction has large errors but it is better than the case where all singular values used (Figure 36b), and is quite accurate in the high frequency range. However, it is inferior to the case where singular values are rejected based on the error band of +/- one standard deviation (Figure 39b).

The force reconstruction for the cases $n_r=6$, $n_e=4$ is shown in Figures 40-42. The force reconstruction improves considerably for all singular values used (compare Figures 40 and 36) and singular value rejection based on +/- one standard deviation in accelerance estimation (compare Figures 42 and 39). The improvement in the force reconstruction is

insignificant when singular values are rejected based on the error band of +/- 3 standard deviation (compare Figures 41 and 37).

The reconstructed forces for n_r=6, n_e=6 are shown in Figures 43-45. The above conclusions remain valid for these cases as well.

In general, as in the previous section, the force reconstruction is always inferior with a large noise amplitude compared to the rather small amplitude used in [5].

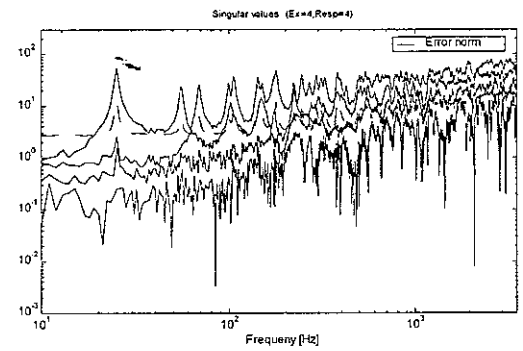

Figure 36a. Singular values along with error norm of accelerance matrix for 4 sources and 4 responses - noise constant with frequency

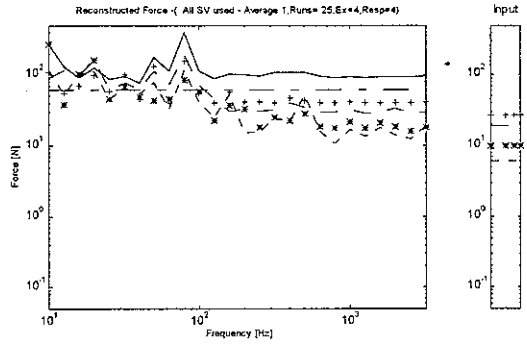

Figure 36b. 1/3 octave band reconstructed forces for 4 sources and 4 responses with all singular - noise constant with frequency

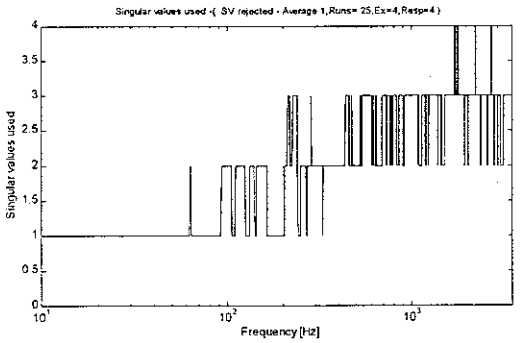

Figure 37a. Number of Singular values used at each frequency for 4 sources and 4 responses. Singular values rejected based on the error band of +/- 3 std. deviation in accelerance estimation - noise constant with frequency

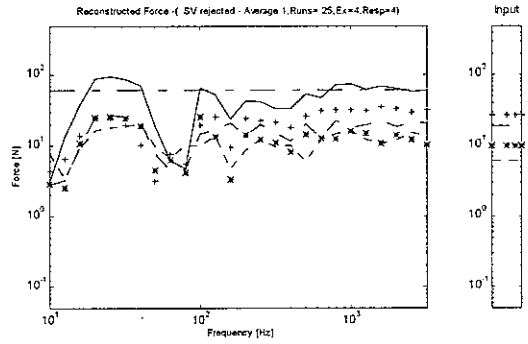

Figure 37b. 1/3 octave band reconstructed forces for 4 sources and 4 responses. Singular values rejected based on the error band of +/- 3 std. deviation in accelerance estimation - noise constant with frequency

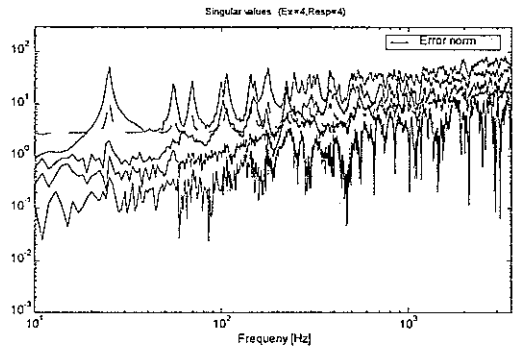

Figure 38a. Singular values along with error norm of accelerance matrix for 4 sources and 4 responses - noise constant with frequency

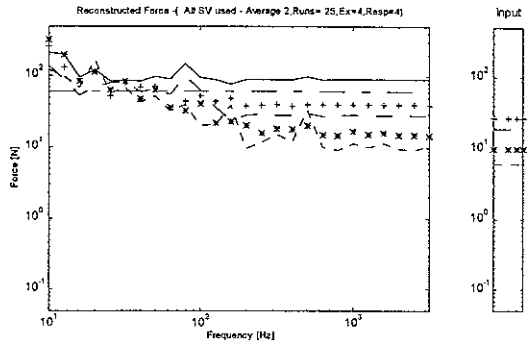

Figure 38b. 1/3 octave band reconstructed forces for 4 sources and 4 responses with all singular and resampling- noise constant with frequency

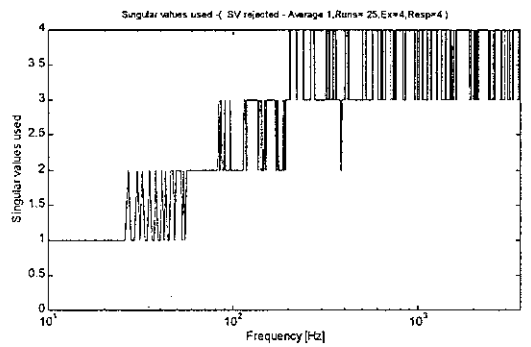

Figure 39a. Number of Singular values used at each frequency for 4 sources and 4 responses. Singular values rejected based on the error band of +/- one std. deviation in accelerance estimation - noise constant with frequency

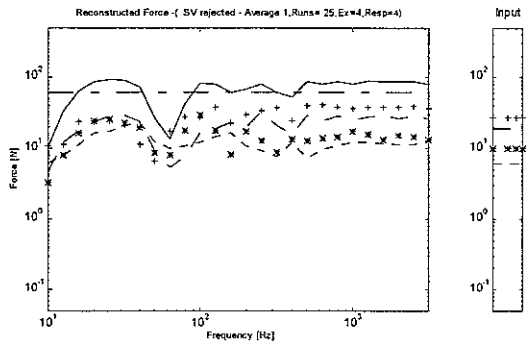

Figure 39b. 1/3 octave band reconstructed forces for 4 sources and 4 responses. Singular values rejected based on the error band of +/- one std. deviation in accelerance estimation - noise constant with frequency

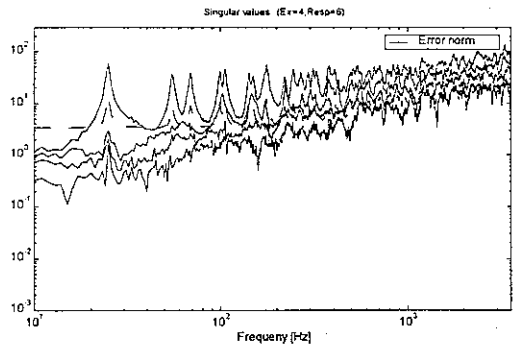

Figure 40a. Singular values along with error norm of accelerance matrix for 4 sources and 6 responses - noise constant with frequency

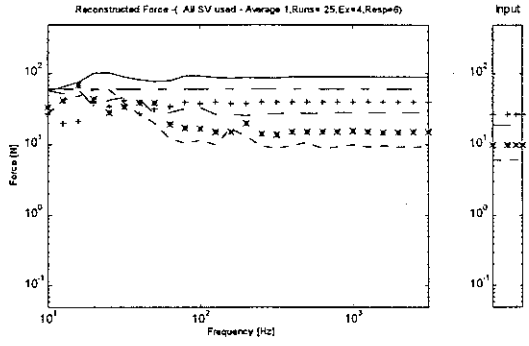

Figure 40b. 1/3 octave band reconstructed forces for 4 sources and 6 responses with all singular - noise constant with frequency

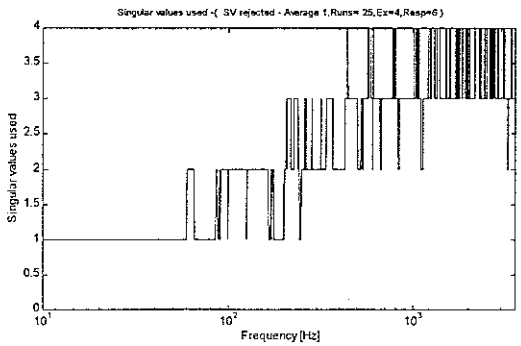

Figure 41a. Number of Singular values used at each frequency for 4 sources and 6 responses. Singular values rejected based on the error band of +/- 3 std. deviation in accelerance estimation - noise constant with frequency

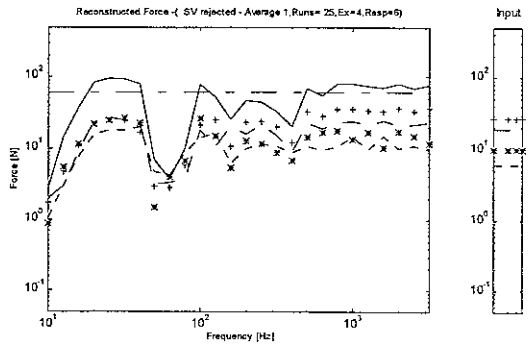

Figure 41b. 1/3 octave band reconstructed forces for 4 sources and 6 responses. Singular values rejected based on the error band of +/- 3 std. deviation in accelerance estimation - noise constant with frequency

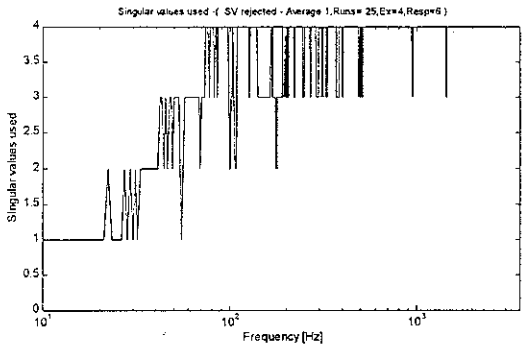

Figure 42a. Number of Singular values used at each frequency for 4 sources and 6 responses. Singular values rejected based on the error band of +/- one std. deviation in accelerance estimation - noise constant with frequency

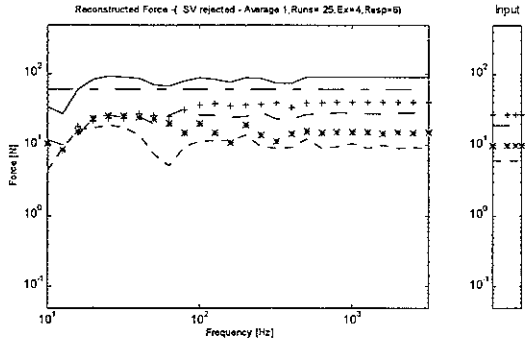

Figure 42b. 1/3 octave band reconstructed forces for 4 sources and 6 responses. Singular values rejected based on the error band of +/- one std. deviation in accelerance estimation - noise constant with frequency

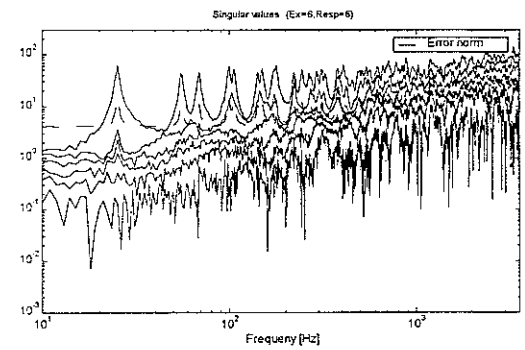

Figure 43a. Singular values along with error norm of accelerance matrix for 6 sources and 6 responses - noise constant with frequency

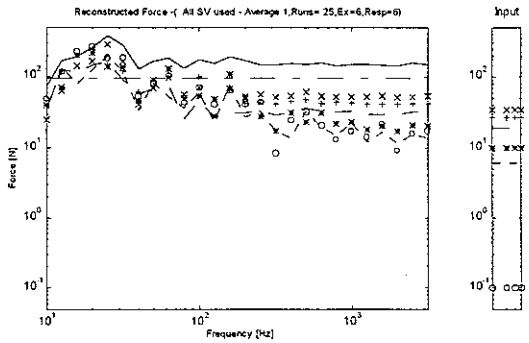

Figure 43b. 1/3 octave band reconstructed forces for 6 sources and 6 responses with all singular - noise constant with frequency

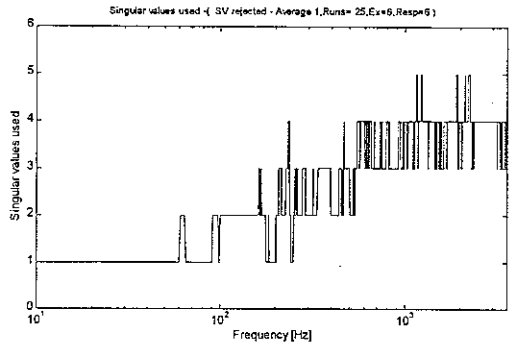

Figure 44a. Number of Singular values used at each frequency for 6 sources and 6 responses. Singular values rejected based on the error band of +/- 3 std. deviation in accelerance estimation - noise constant with frequency

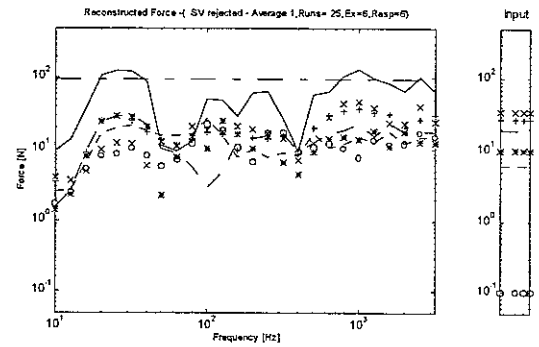

Figure 44b. 1/3 octave band reconstructed forces for 6 sources and 6 responses. Singular values rejected based on the error band of +/- 3 std. deviation in accelerance estimation - noise constant with frequency

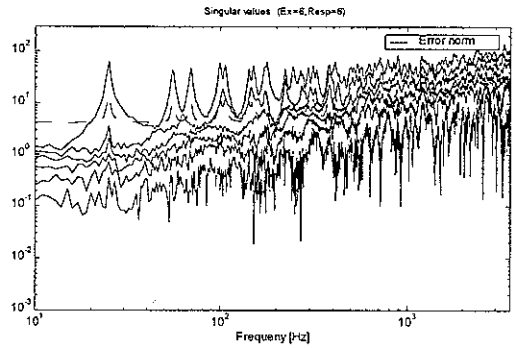

Figure 45a. Singular values along with error norm of accelerance matrix for 6 sources and 6 responses - noise constant with frequency

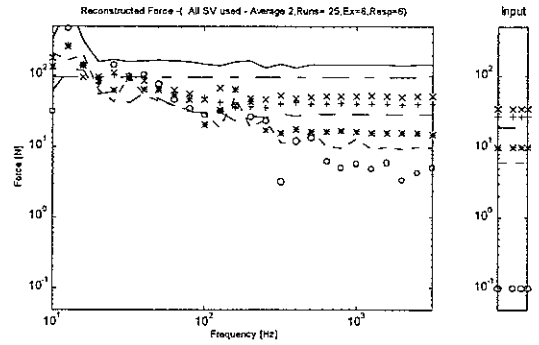

Figure 45b. 1/3 octave band reconstructed forces for 6 sources and 6 responses with all singular and resampling - noise constant with frequency

3.6 Velocity at the receiver location

Figures 46a-d show the 1/3 octave band velocity response at the receiver location for $n_r=n_e=4$. The velocity response predicted at lower frequencies with all singular values used is quite poor whether or not phase information is used in the averaging process, as shown in Figures 46a-b. The response is accurate only in the vicinity of the first mode of the rectangular plate.

The results when singular values are rejected based on the error band of +/- 3 standard deviation are shown in Figures 46c-d. In comparison with the case where all singular values are used (Figure 46a-b) the prediction at the receiver location has improved considerably. However the velocity prediction in the region from 40 to 100 Hz is poor (as were the forces). The velocity response improves further when singular values are rejected based on the error band of +/- one standard deviation in the estimation of accelerance as shown in the Figures 46g-h. The resampling strategy results in large prediction errors compared to singular value rejection (Figures 46e-f and 46g-h). The resampling strategy is thus observed to be very sensitive to the amplitude of corrupting noise as found in the earlier section. As with the force reconstruction, the velocity prediction improves significantly for averaging with phase information when a large number of averages are taken (200 rather than 25). The singular value rejection strategy is least sensitive to the noise amplitude, although the results differ considerably based on the size of the error band used in constructing the error matrix.

The velocity prediction improves for an overdetermined system (n_r=6, n_e=4) as shown in Figures 47a-b for all singular values used (compare with 46a-b).

For the case of n_r=6, n_e=6 results are shown in Figures 48a-c. In this case the low frequency prediction improves for all the cases (compare Figures 48 and 46). The singular value rejection method, again, gives the best prediction (Figure 48c-d).

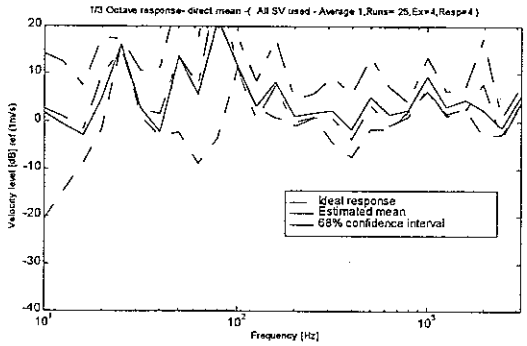

Figure 46a. 1/3 octave band velocity response for 4 sources and 4 responses with all singular values used (with phase information) - noise constant with frequency

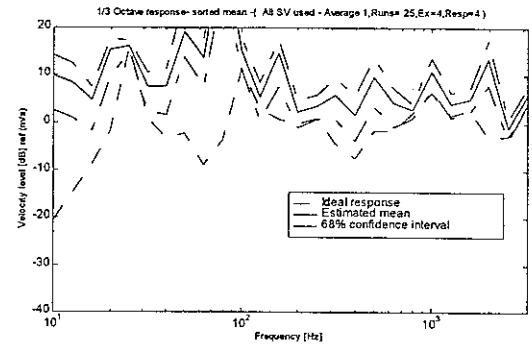

Figure 46b. 1/3 octave band velocity response for 4 sources and 4 responses with all singular values used (no phase information) - noise constant with frequency

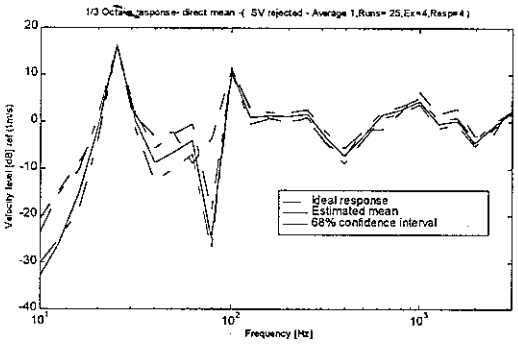

Figure 46c. 1/3 octave band velocity response for 4 sources and 4 responses with singular value rejection based on error band of +/- 3 std. deviation in accelerance (with phase information) - noise constant with frequency

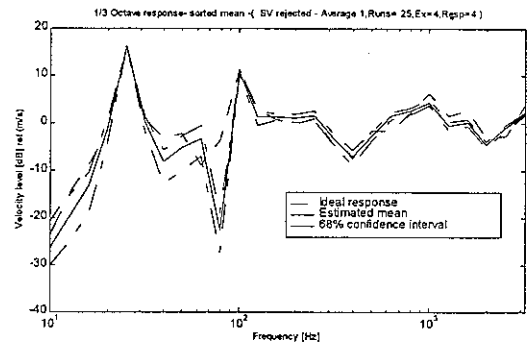

Figure 46d. 1/3 octave band velocity response for 4 sources and 4 responses with singular value rejection based on error band of +/- one std. deviation in accelerance (with phase information) - noise constant with frequency

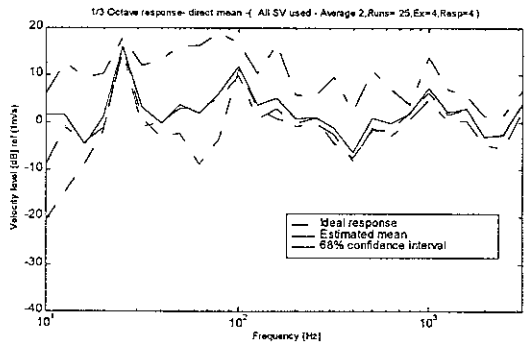

Figure 46e. 1/3 octave band velocity response for 4 sources and 4 responses with all singular values used and resampling (with phase information) - noise constant with frequency

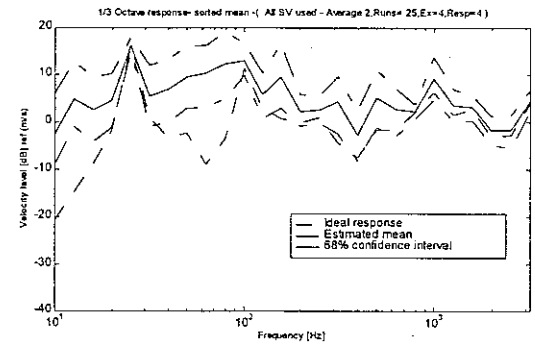

Figure 46f. 1/3 octave band velocity response for 4 sources and 4 responses with all singular values used and resampling (no phase information) - noise constant with frequency

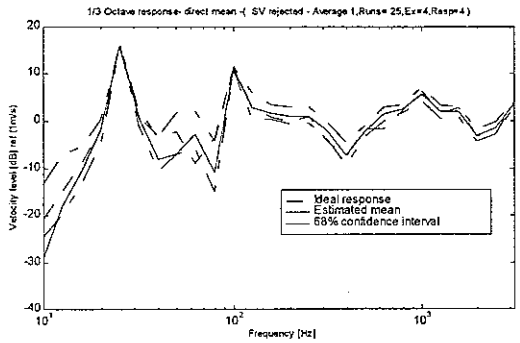

Figure 46g. 1/3 octave band velocity response for 4 sources and 4 responses with singular value rejection based on error band of +/- one std. deviation in accelerance (with phase information) - noise constant with frequency

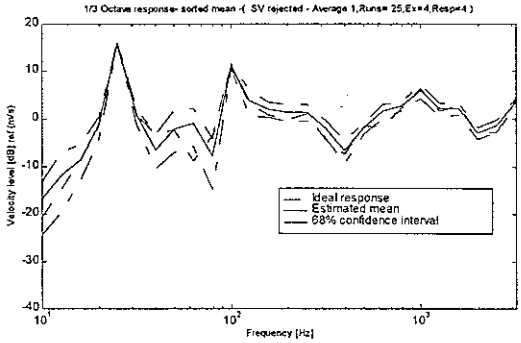

Figure 46h. 1/3 octave band velocity response for 4 sources and 4 responses with singular value rejection based on error band of +/- one std. deviation in accelerance (no phase information) - noise constant with frequency

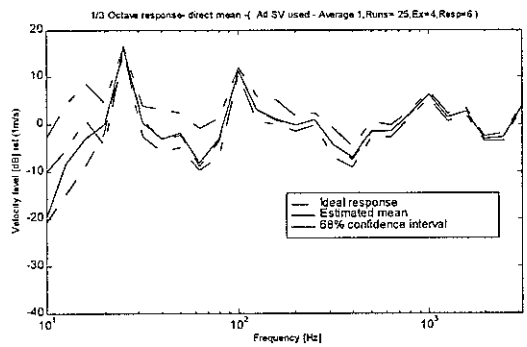

Figure 47a. 1/3 octave band velocity response for 4 sources and 6 responses with all singular values used (with phase information) - noise constant with frequency

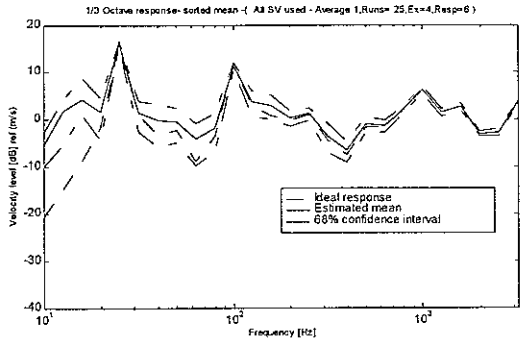

Figure 47b. 1/3 octave band velocity response for 4 sources and 6 responses with all singular values used (no phase information) - noise constant with frequency

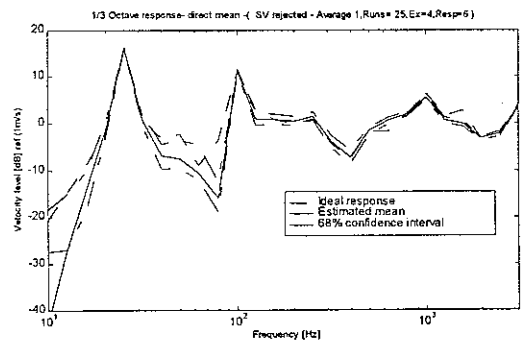

Figure 47c. 1/3 octave band velocity response for 4 sources and 6 responses with singular value rejection based on error band of +/- 3 std. deviation in accelerance (with phase information) - noise constant with frequency

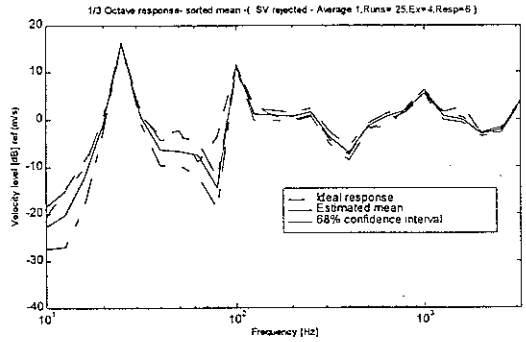

Figure 47d. 1/3 octave band velocity response for 4 sources and 6 responses with singular value rejection based on error band of +/- 3 std. deviation in accelerance (no phase information) - noise constant with frequency

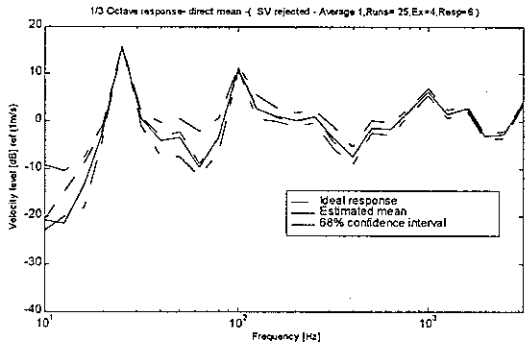

Figure 47e. 1/3 octave band velocity response for 4 sources and 6 responses with singular value rejection based on error band of +/- onr std. deviation in accelerance (with phase information) - noise constant with frequency

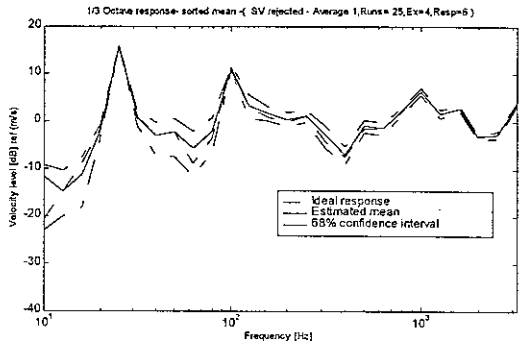

Figure 47f. 1/3 octave band velocity response for 4 sources and 6 responses with singular value rejection based on error band of +/- onr std. deviation in accelerance (with phase information) - noise constant with frequency

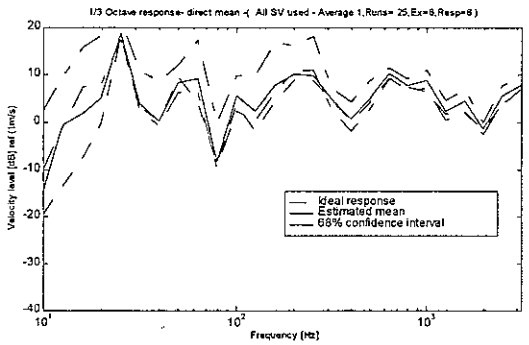

Figure 48a. 1/3 octave band velocity response for 6 sources and 6 responses with all singular values used (with phase information) - noise constant with frequency

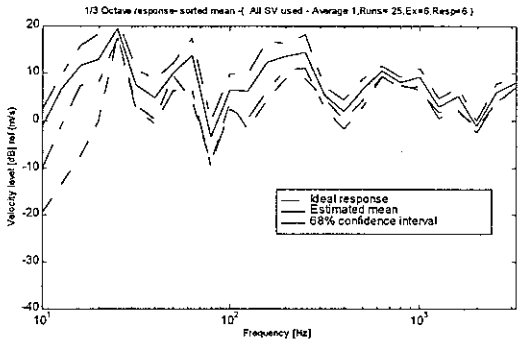

Figure 48b. 1/3 octave band velocity response for 6 sources and 6 responses with all singular values used (no phase information) - noise constant with frequency

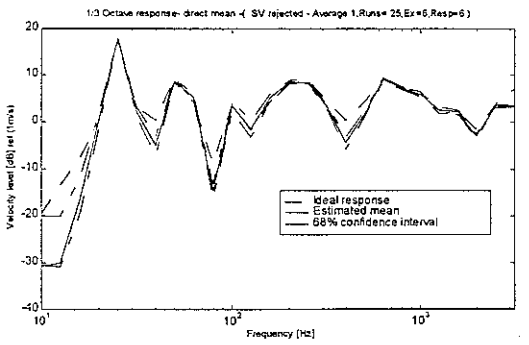

Figure 48c. 1/3 octave band velocity response for 6 sources and 6 responses with singular value rejection based on error band of +/- 3 std. deviation in accelerance (with phase information) - noise constant with frequency

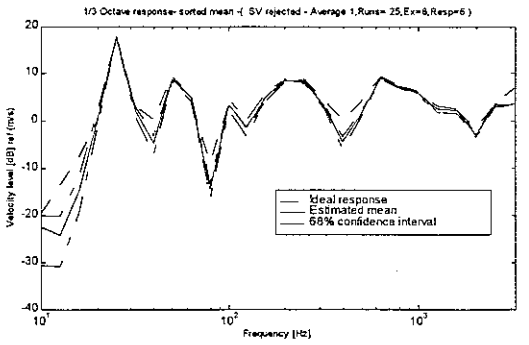

Figure 48d. 1/3 octave band velocity response for 6 sources and 6 responses with singular value rejection based on error band of +/- 3 std. deviation in accelerance (no phase information) - noise constant with frequency

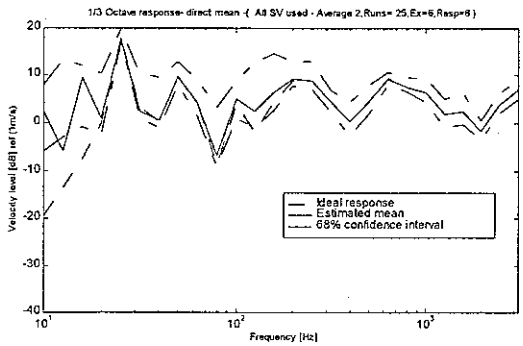

Figure 48e. 1/3 octave band velocity response for 6 sources and 6 responses with all singular values used and resampling(with phase information) - noise constant with frequency

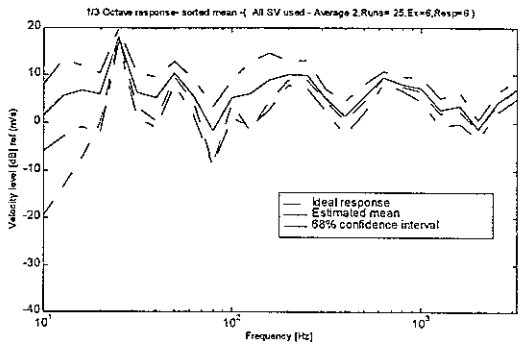

Figure 48f. 1/3 octave band velocity response for 6 sources and 6 responses with all singular values used and resampling(no phase information) - noise constant with frequency

3.7 Conclusions

The conclusions drawn in [5] should be modified slightly when considerably large corrupting noise is introduced in the simulations representing the experimental 'measurements'. Under these circumstances, singular value rejection results in more reliable predictions than resampling of the accelerance matrix (although, resampling predictions can be improved by using a larger number of averages). In general it is observed that the errors in the force reconstruction and the velocity prediction are large in the frequency range from 40 to 100Hz where few modes are present. It does not improve even when singular values rejection is applied.

4. The effect of a proportional noise model

4.1 Introduction

In [5] while simulating the conditions to represent the experiments, Gaussian noise models with constant amplitude and amplitude proportional to frequency were used. In chapter 3 those models have been studied with increased amplitude. In all these studies, to estimate the measured accelerances, the corrupting noise is introduced in acceleration and force 'measurements'. In general it has been observed that the error in accelerance estimation can be better represented by an error model which is proportional to the accelerance amplitude [7]. In this chapter the sensitivity of the different strategies to this noise model is studied.

The noise model used here can be represented as below. For the accelerance the noise is taken as

$$E = |A|\varepsilon . N_1 e^{j2\pi N_2}$$

where A - theoretical accelerance matrix [5]

ε - Mean error ratio

N_1 - Random numbers of 0 mean and variance 1 with normal distribution

N_2 - Random numbers from 0 to 1 with uniform distribution

Similarly, noise in acceleration measurement is given by

$$a_E = |A| f\varepsilon . N_1 e^{j2\pi N_2}$$

where f - is a force vector

In this study, ε is taken to be 0.2.

4.2 Force reconstruction

Figures 49a-b show the singular values of the accelerance matrix and the reconstructed forces for n_r=n_e=4 when all singular values are used. The force reconstruction is poor at many of the frequencies. Figures 50a-b show the number of singular values used at each frequency and the forces reconstructed when singular values are rejected based on the threshold established by the norm of accelerance error matrix constructed from the band of +/- 3 standard deviation in the estimation of accelerance. The forces are under-estimated at most of the frequencies. When singular values are rejected based on the error band of +/- one standard deviation in the accelerance estimation (Figures 52a-b), the force reconstruction improves across the entire frequency range. However, the force reconstruction remains poor in the frequency range from 40 to 100 Hz. Figures 51a-b show the results for resampling of the accelerance matrix. The force reconstruction is incorrect but it is better than the cases where all singular values are used (Figure 49b). However, it is slightly inferior to the case where singular values are rejected based on the error band of +/- one standard deviation.

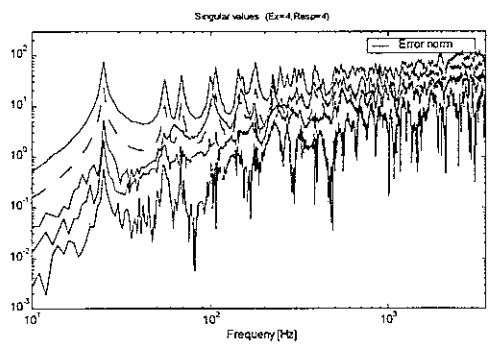

Figure 49a. Singular values along with error norm of accelerance matrix for 4 sources and 4 responses - Proportional noise model

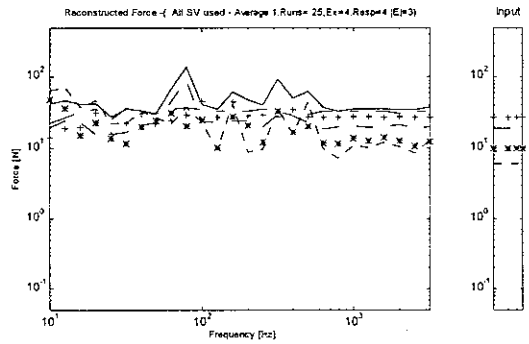

Figure 49b. 1/3 octave band reconstructed forces for 4 sources and 4 responses with all singular - Proportional noise model

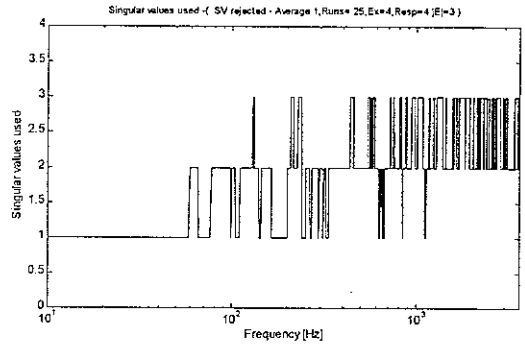

Figure 50a. Number of Singular values used at each frequency for 4 sources and 4 responses. Singular values rejected based on the error band of +/- 3 std. deviation in accelerance estimation - Proportional noise model

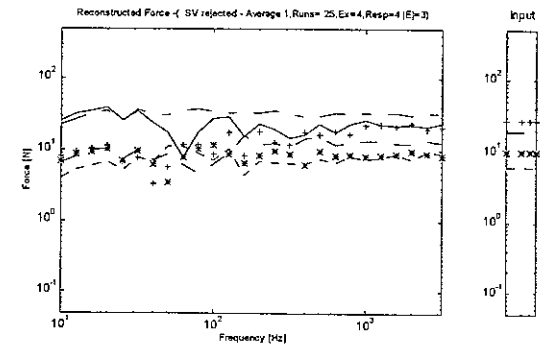

Figure 50b. 1/3 octave band reconstructed forces for 4 sources and 4 responses. Singular values rejected based on the error band of +/- 3 std. deviation in accelerance estimation - Proportional noise model

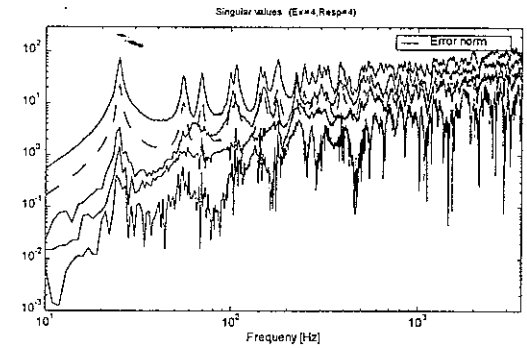

Figure 51a. Singular values along with error norm of accelerance matrix for 4 sources and 4 responses - Proportional noise model

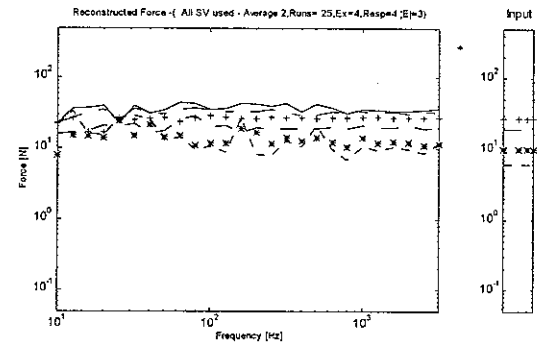

Figure 51b. 1/3 octave band reconstructed forces for 4 sources and 4 responses with all singular values used and resampling- Proportional noise model

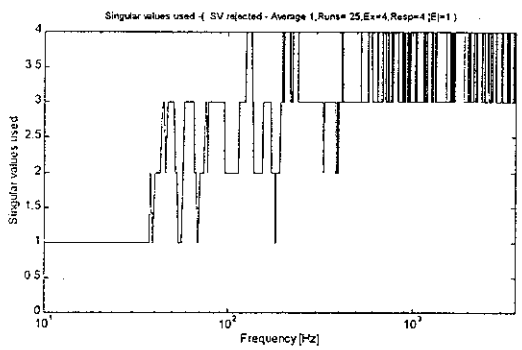

Figure 52a. Number of Singular values used at each frequency for 4 sources and 4 responses. Singular values rejected based on the error band of +/- one std. deviation in accelerance estimation - Proportional noise model

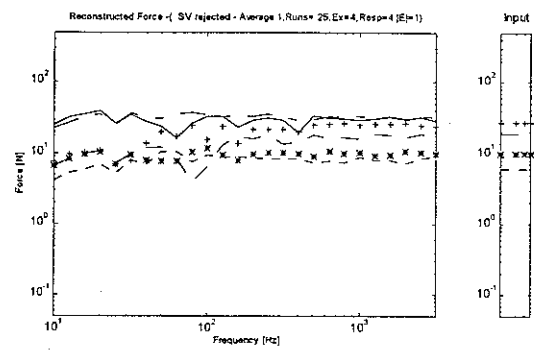

Figure 52b. 1/3 octave band reconstructed forces for 4 sources and 4 responses. Singular values rejected based on the error band of +/- one std. deviation in accelerance estimation - Proportional noise model

4.3 Velocity at the receiver location

Figures 53a-h show the 1/3 octave band velocity responses at the receiver location for $n_r=n_e=4$. The velocity response predicted with all singular values used is incorrect whether or not phase information is used in the averaging process as shown in Figures 53a-b.

The results obtained when singular values are rejected based on the error band of +/- 3 standard deviations are shown in Figures 53c-d. In comparison with the case where all singular values are used, the prediction at the receiver location has improved considerably. However the velocity prediction in the region from 30 to 100 Hz is incorrect. The velocity response improves further when singular values are rejected based on the error band of +/- one standard deviation in the estimation of accelerance as shown in Figures 53g-h. The resampling strategy results in better predictions than singular value rejection when phase information is used for averaging (Figures 53e-f and 53c-d, 53e-f). The resampling and singular value rejection strategy based on +/- one standard deviation are found to be least sensitive to the proportional noise model while predicting the velocity response (compare with [5]).

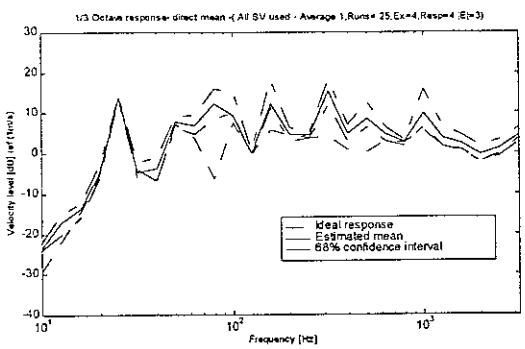

Figure 53a. 1/3 octave band velocity response for 4 sources and 4 responses with all singular values used (with phase information) - Proportional noise model

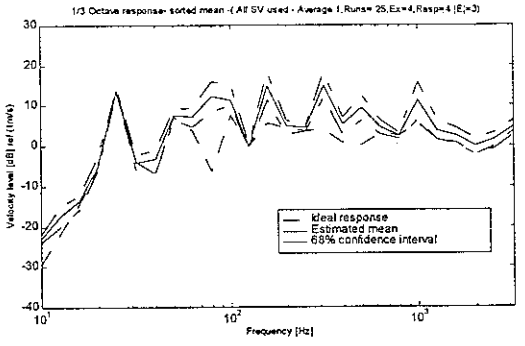

Figure 50b. 1/3 octave band velocity response for 4 sources and 4 responses with all singular values used (no phase information) - Proportional noise model

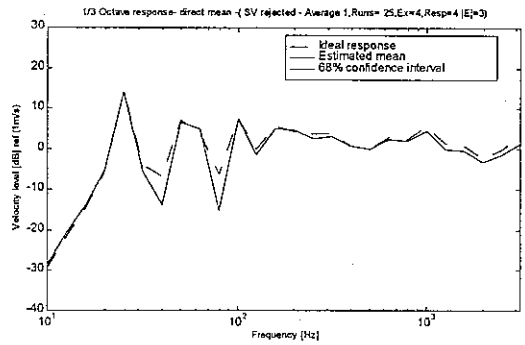

Figure 53c. 1/3 octave band velocity response for 4 sources and 4 responses with singular value rejection based on error band of +/- 3 std. deviation in accelerance (with phase information) - Proportional noise model

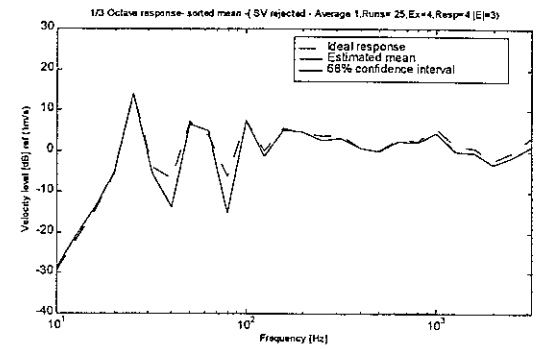

Figure 53d. 1/3 octave band velocity response for 4 sources and 4 responses with singular value rejection based on error band of +/- 3 std. deviation in accelerance (no phase information) - Proportional noise model

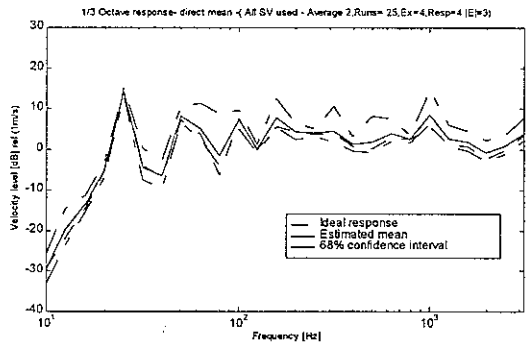

Figure 53e. 1/3 octave band velocity response for 4 sources and 4 responses with all singular values used and resampling (with phase information) - Proportional noise model

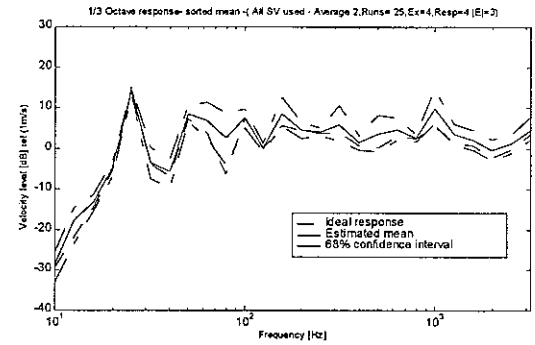

Figure 53f. 1/3 octave band velocity response for 4 sources and 4 responses with all singular values used and resampling (no phase information) - Proportional noise model

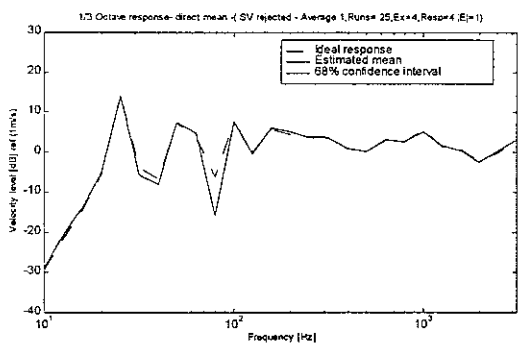

Figure 53g. 1/3 octave band velocity response for 4 sources and 4 responses with singular value rejection based on error band of +/- one std. deviation in accelerance (with phase information) - Proportional noise model

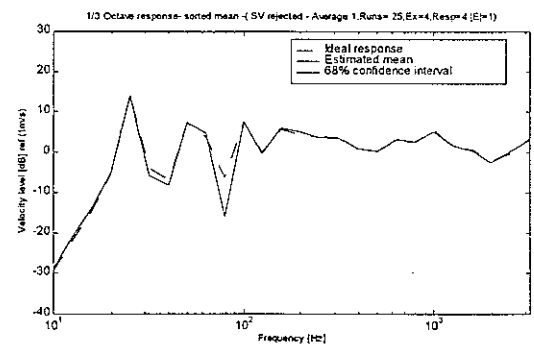

Figure 53h. 1/3 octave band velocity response for 4 sources and 4 responses with singular value rejection based on error band of +/- one std. deviation in accelerance (no phase information) - Proportional noise model

4.4 Conclusion

In general, all the strategies are found to give better results when a proportional Gaussian noise model is used for corrupting the 'measured' accelerance compared to when a Gaussian addititive model (both small or large amplitude). The singular value rejection and the resampling strategies result in reliable predictions for this noise model.

5. Singular value rejection based on errors in operational accelerations

5.1 Introduction

An improved force identication is achieved in ref [5] by the rejection of these singular values which are small enough to be influenced by measurement noise. This rejection is based on the threshold established by the norm of the accelerance error matrix. As discussed earlier, the results obtained from this strategy are dependent on the band of error used i.e +/- one or three standard deviation. However, the improvement is not so significant at frequencies in the vicinity of antiresonance, particularly in the region 40-80Hz (see Figures 23, 26, 30g-h, 39, 46g-h). It is interesting to explore a second criterion [8] for rejecting the singular values, based on their contribution to the operational response. The operational responses are the summation of contributions from each of the singular values. In this criterion smaller singular values are rejected if they contribute less than the error in the measurement of operational accelerations. The errors in the operational responses can be estimated based on a covariance matrix recorded during the measurments or by using relations as in [7]. The formulation for this strategy is given below

5.2 Formulation

From [7], the variance (squared standard deviation) in the estimation of the auto-spectrum S_{xx} is given by

$$Var\left[\hat{S}_{xx}\right] = \frac{\left|\hat{S}_{xx}\right|}{n_S} \qquad (1)$$

where n_s is the number of samples taken.

From the accelerance matrix, if the forces are known, the acceleration can be calculated as

$$\{a\} = [A]\{f\}$$

Due to the errors in the measurement, the measured acceleration can be represented as

$$\left\{\hat{a}\right\} = \{a + a_e\} \qquad (2)$$

The contribution from each singular value to the operational responses can be derived as below

Using singular value decomposition, the accelerance matrix can be decomposed as

$$\hat{A} = USV^H$$

This can also be written as

$$\hat{A} = A_1 + A_2 + A_3 ..... + A_{n_e}$$

where

$$A_j = U_{i,j} S_{j,j} V^H_{j,k} \qquad \text{for j,k=1.....} n_e \qquad \text{and i=1.....} n_r \qquad (3)$$

The contribution from each singular value the response is given by

$$\{a_j\} = [A_j]\{f\} \qquad \text{for j=1.....} n_e \qquad (4)$$

The equation (4) cannot be evaluated since the forces are not known. However this difficulty can be overcome by normalisation. The contribution from the largest singular value can be taken as a first approximation to the acceleration response. Therefore

$$\{a_f\} \approx [A_1]\{f\}$$

where a_f is a first approximation to the acceleration response

Taking the norm of the above equation

$$\left\|\{a_f\}\right\| \approx \left\|[A_1]\{f\}\right\|$$

$$\left\|\{a_f\}\right\| \leq \left\|[A_1]\right\| \left\|\{f\}\right\| \tag{5}$$

Taking the norm of (4)

$$\left\|\{a_j\}\right\| = \left\|[A_j]\{f\}\right\| \qquad \text{for j=1.....}n_e$$

$$\left\|\{a_j\}\right\| \leq \left\|[A_j]\right\| \left\|\{f\}\right\| \tag{6}$$

Taking the ratio of (5) and (6), although they are both inequalities, gives the qualitative relation

$$\frac{\left\|\{a_j\}\right\|}{\left\|\{a_f\}\right\|} \sim \frac{\left\|[A_j]\right\|}{\left\|[A_1]\right\|} \tag{7}$$

The above relation, for 2-norm, can be written as

$$\frac{\left\|\{a_j\}\right\|}{\left\|\{a_f\}\right\|} \sim \frac{S_j}{S_1} \tag{8}$$

This suggests that singular values should be rejected when

$$\frac{\left\|\{a_e\}\right\|}{\left\|\{a\}\right\|} \geq \frac{\left\|\{a_j\}\right\|}{\left\|\{a_f\}\right\|} \qquad \text{OR} \qquad \geq \frac{S_j}{S_1} \tag{9}$$

5.3 Cumulative sum of singular values

In the earlier study [5], as in equation (9), individual singular values were compared to the norm of the error matrix which may reject more information than necessary. Hence it

is interesting to investigate the effect of comparing individual singular values or the cumulative sum of singular values while rejecting the singular values. The formulation for this criterion is discussed below.

Let the partial contribution from last (n_e-r) singular values to the accelerations be given by

$$\left\{a_{partial}\right\} = \left[A_r + A_{r+1} \ldots\ldots + A_{n_e}\right]\{f\} \tag{10}$$

Taking the norm of the above equation

$$\left\|\left\{a_{partial}\right\}\right\| = \left\|\left[A_r + A_{r+1} \ldots\ldots + A_{n_e}\right]\{f\}\right\|$$

$$\left\|\left\{a_{partial}\right\}\right\| \le \left(\|A_r\| + \|A_{r+1}\| \ldots + \|A_{n_e}\|\right)\|\{f\}\| \tag{11}$$

Taking the ratio of relation (5) and (11) gives the qualitative relation

$$\frac{\left\|\left\{a_{partial}\right\}\right\|}{\left\|\left\{a_f\right\}\right\|} \sim \frac{\left(\|A_r\| + \|A_{r+1}\| \ldots + \|A_{n_e}\|\right)\|\{f\}\|}{\|[A_1]\|\|\{f\}\|} \tag{12}$$

The above relation, for 2-norm, can be written as

$$\frac{\left\|\left\{a_{partial}\right\}\right\|}{\left\|\left\{a_f\right\}\right\|} \sim \frac{S_r + S_{r+1} \ldots + S_{n_e}}{S_1}$$

This suggests that the contribution from last (n_e-r) singular values can be neglected when

$$\frac{\left\|\left\{a_e\right\}\right\|}{\|\{a\}\|} \ge \frac{\left\|\left\{a_{partial}\right\}\right\|}{\left\|\left\{a_f\right\}\right\|} \quad \text{OR} \quad \ge \frac{S_r + S_{r+1} \ldots + S_{n_e}}{S_1} \tag{13}$$

The same argument can be extended for using cumulative singular value summation for the rejection of singular values based on the norm of accelerance error matrix.

If, instead of the 2-norm, the Frobenius norm is used then there is no necessity to consider the cumulative effect of singular values. This is because the Frobenius norm of a matrix is given by

$\|[A]\|_F = \sqrt{S_1 + \ldots\ldots + S_{n_e}}$ which considers all singular values.

The following four cases are compared in this section

1. Singular value rejection based on the norm of the acceleration error
    a. Comparing individual singular values with and without resampling
    b. Comparing cumulative sum of singular values
2. Singular value rejection based on the norm of the accelerance error matrix
    a. Comparing individual singular values
    b. Comparing cumulative sum of singular values

The noise model used is same as in section 3.1 and it has same amplitude as there.

5.4 Force reconstruction

Figures 54a-b show number of the singular values used at each frequency and the forces reconstructed when singular values are rejected based on the threshold established by the norm of the operational acceleration error vector. This is constructed from the band of +/- one standard deviation in the measurement of acceleration and is for $n_r=n_e=4$. In this case individual singular values are compared with the error norm. The forces are slightly overestimated at most of the frequencies. When the cumulative sum of singular values is compared with the error norm, the force reconstruction does not improve significantly (compare Figures 54 and 55). Figures 56a-b show the results for resampling along with singular value rejection (individual singular values compared). The force reconstruction does not differ significantly from the above cases.

When singular values are rejected based on the norm of the error matrix constructed from +/- 3 standard deviation band in the estimation of accelerance, the force reconstruction is very poor (Figure 57). As in the earlier experiments, the force reconstruction improves when +/- one standard deviation band is used (compare Figures 58 and 57). Figure 59 shows the force reconstruction when the cumulative contribution of singular values is considered rather than individual singular values. From Figures 59a and 58a it is seen that more singular values are used in the low and high frequency ranges when the cumulative sum is considered. The force reconstruction also shows a difference in that the amplitudes of the forces are larger to some extent when based on the cumulative sum.

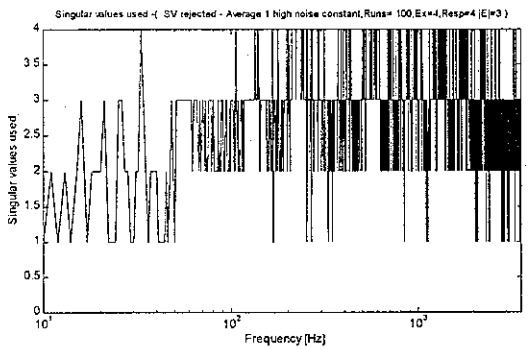

Figure 54a. Number of Singular values used at each frequency for 4 sources and 4 responses. Singular values rejected based on the error band of +/- one std. deviation in operational acceleration

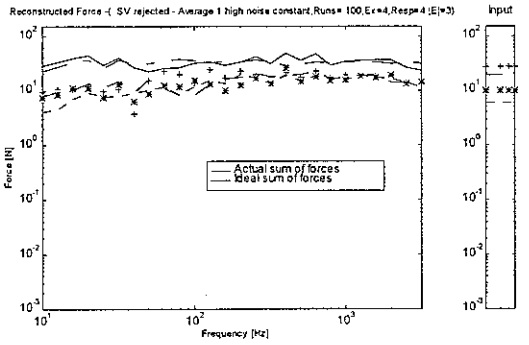

Figure 54b. 1/3 octave band reconstructed forces for 4 sources and 4 responses. Singular values rejected based on the error band of +/- one std. deviation in operational acceleration

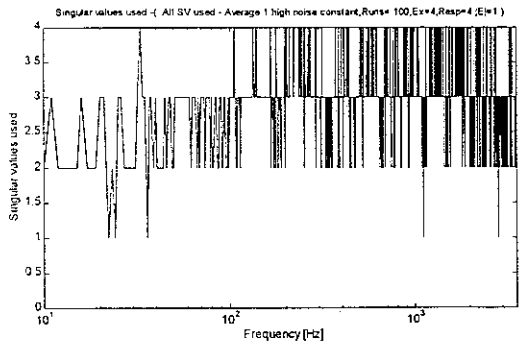

Figure 55a. Number of Singular values used at each frequency for 4 sources and 4 responses. Singular values rejected based on the error band of +/- one std. deviation in operational acceleration. Cumulative contribution from singular values considered.

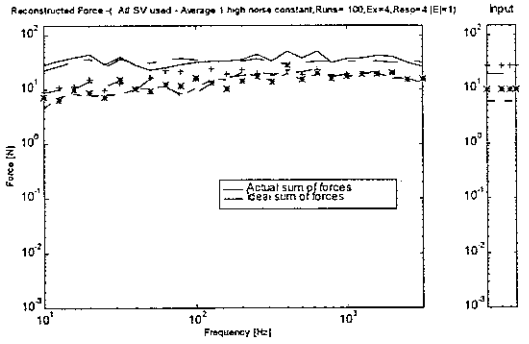

Figure 55b. 1/3 octave band reconstructed forces for 4 sources and 4 responses. Singular values rejected based on the error band of +/- one std. deviation in operational acceleration. Cumulative contribution from singular values considered.

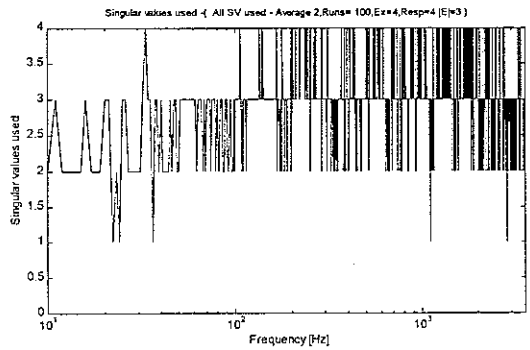

Figure 56a. Number of Singular values used at each frequency for 4 sources and 4 responses. Singular values rejected based on the error band of +/- one std. deviation in operational acceleration and resampling.

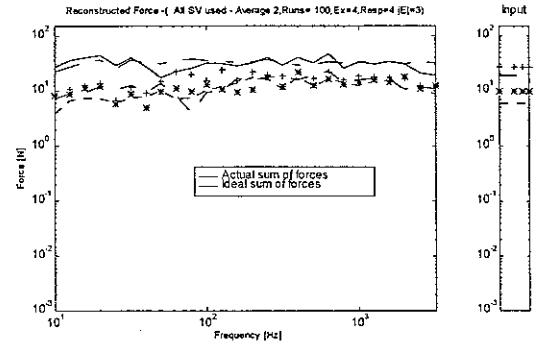

Figure 56b. 1/3 octave band reconstructed forces for 4 sources and 4 responses. Singular values rejected based on the error band of +/- one std. deviation in operational acceleration and resampling.

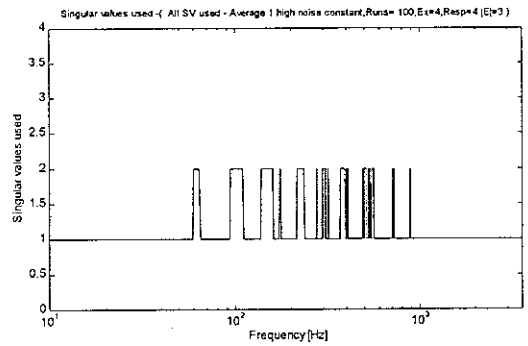

Figure 57a. Number of Singular values used at each frequency for 4 sources and 4 responses. Singular values rejected based on the error band of +/- 3 std. deviation in accelerance estimation.

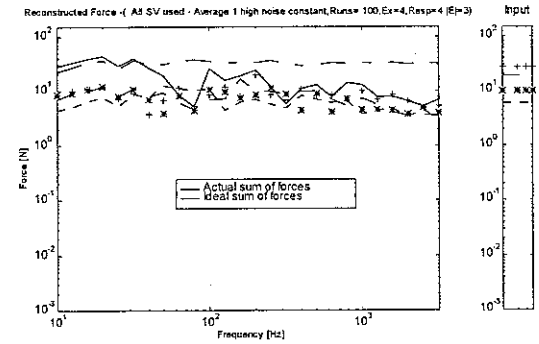

Figure 57b. 1/3 octave band reconstructed forces for 4 sources and 4 responses. Singular values rejected based on the error band of +/- 3 std. deviation in accelerance estimation.

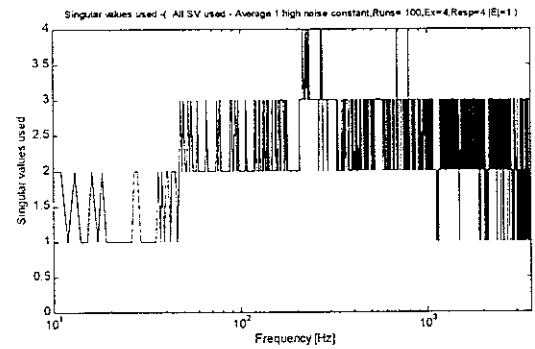

Figure 58a. Number of Singular values used at each frequency for 4 sources and 4 responses. Singular values rejected based on the error band of +/- one std. deviation in accelerance estimation.

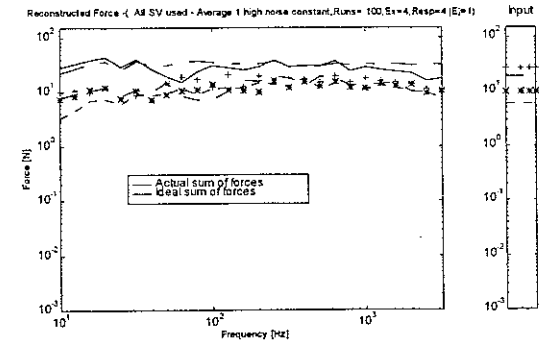

Figure 58b. 1/3 octave band reconstructed forces for 4 sources and 4 responses. Singular values rejected based on the error band of +/- one std. deviation in accelerance estimation.

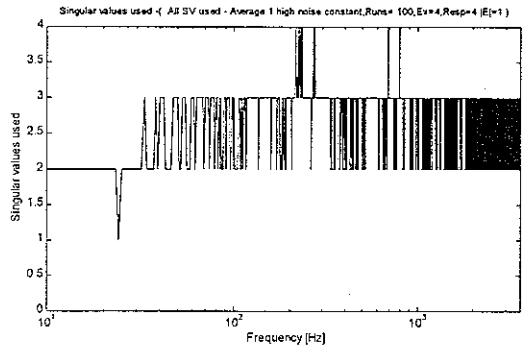

Figure 59a. Number of Singular values used at each frequency for 4 sources and 4 responses. Singular values rejected based on the error band of +/- one std. deviation in accelerance estimation. Cumulative contribution from singular values considered.

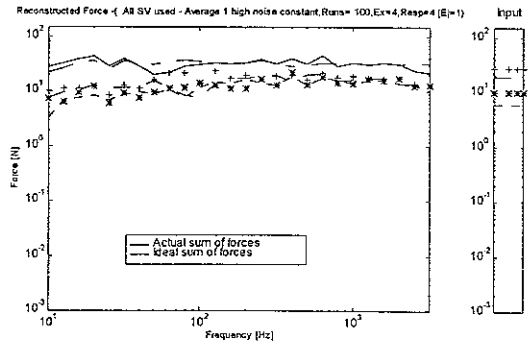

Figure 59b. 1/3 octave band reconstructed forces for 4 sources and 4 responses. Singular values rejected based on the error band of +/- one std. deviation in accelerance estimation. Cumulative contribution from singular values considered.

5.5 Velocity at the receiver location

Figures 60a-f show the 1/3 octave band velocity response at the receiver location for n_r=n_e=4. The velocity response between 30 and 100 Hz is underestimated when singular values are rejected based on the comparison of individual singular values with the norm of the error in the acceleration measurement (Figure 60a). At all other frequencies the predicted response is reasonably accurate. When the cumulative sum of singular values is used in the comparison, the response in the frequency range 30 to 100Hz improves (compare Figures 60b and 60a). Further improvement at higher frequencies is acheived when singular value rejection is combined with resampling (Figure 60c).

The results when singular values are rejected based on the norm of the error in the accelerance are shown in Figure 60d-f. The velocity prediction is very poor for the case where the +/- 3 standard deviation band is used (Figure 60d). The velocity is underestimated at most of the frequencies. When the +/- one standard deviation band is used, the predictions improve considerably (Figure 60e). The response in the frequency range 30 to 100Hz is still underestimated. The velocity response predicted in this region

improves when the cumulative sum of singular values is compared with the error norm (compare Figures 60e and 60f).

5.6 Conclusion

In general, predictions by both methods (norm based on the acceleration error and the accelerance error) are reliable when the norm is based on the +/- one standard deviation error band. In the case of the acceleration error, further improvements are achieved by resampling and using the cumulative sum of the smallest singular values. For the case of the accelerance error, good improvement is observed when the cumulative sum is taken for comparing with the error norm. Hence, singular values have to be rejected based on a comparison of the error norm with the cumulative sum of singular values.

The above conclusions depend on the amplitude of corrupting noise used. It might be possible to get better predictions with noisy accelerance using accelerance error based singular value rejection. On the other hand for noisy accelerations acceleration error based singular value rejection might suit.

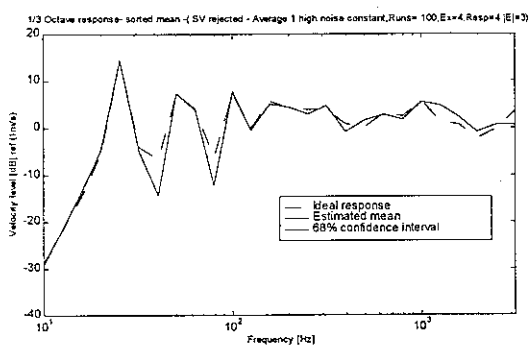

Figure 60a. 1/3 octave band velocity response for 4 sources and 4 responses with singular value rejection based on error band of +/- one std. deviation in operational acceleration.

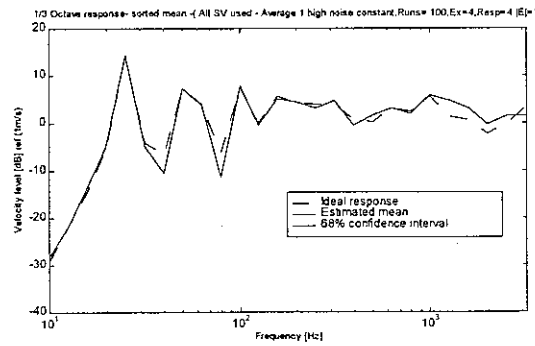

Figure 60b. 1/3 octave band velocity response for 4 sources and 4 responses with singular value rejection based on error band of +/- one std. deviation in operational acceleration. Cumulative contribution from singular values considered.

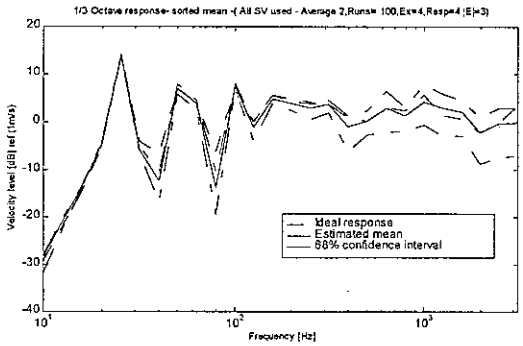

Figure 60c. 1/3 octave band velocity response for 4 sources and 4 responses with singular value rejection based on error band of +/- one std. deviation in operational acceleration and resampling.

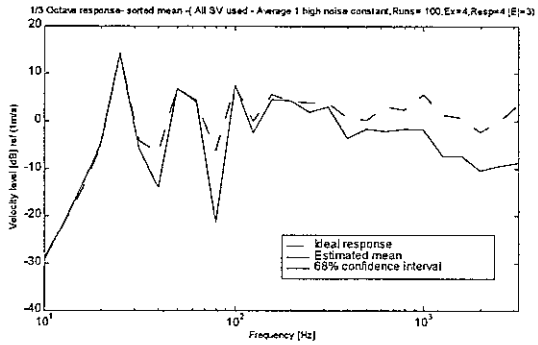

Figure 60d. 1/3 octave band velocity response for 4 sources and 4 responses with singular value rejection based on error band of +/- 3 std. deviation in accelerance estimation.

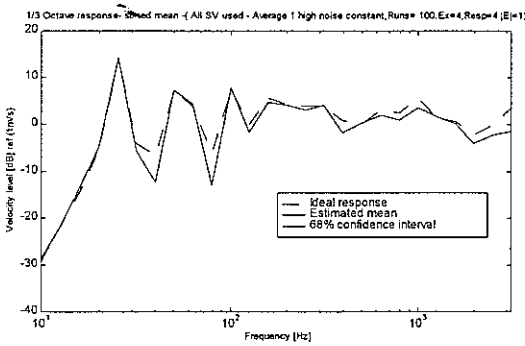

Figure 60e. 1/3 octave band velocity response for 4 sources and 4 responses with singular value rejection based on error band of +/- one std. deviation in accelerance estimation.

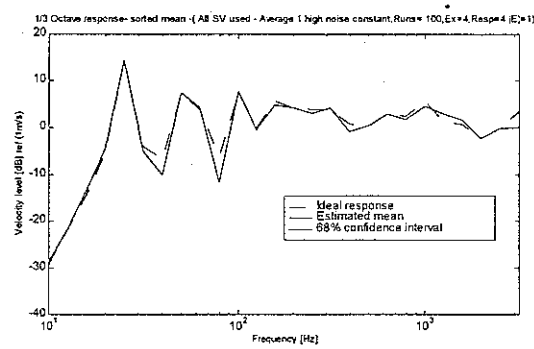

Figure 60f. 1/3 octave band velocity response for 4 sources and 4 responses with singular value rejection based on error band of +/- one std. deviation in accelerance estimation. Cumulative contributions considered.

6. Force identification with different FRF estimators

In the work up to now the frequency response function estimator H_1 has been used. This is designed to minimise the effect of noise on the output signal. H_1 is the most popular frequency response function estimator. It is quite accurate at antiresonance. However, it underestimates the FRF near the resonance (in fact it underestimates the FRF at all frequencies but the difference is small apart from near resonances). As observed in [5] small errors at resonance (when there is a high condition number of the accelerance matrix) can lead to large force reconstruction errors. To overcome this it might be helpful to use an alternative FRF estimator, such as the H_2 estimator which is accurate near the resonances. It is also interesting to explore other estimators which combine the advantages of the H_1 and H_2 estimators. Five different estimators are used in this chapter to reconstruct the forces, and the results from each are compared. These estimators are described in Appendix. The corrupting noise model used in this section is similar to the one used in section 3.4 which has constant amplitude for all frequencies.

6.1 Frequency response estimators

Figures 61b-c show the transfer accelerance from forcing point 1 to response point 1 obtained using H_1. This estimator almost matches the theoretical accelerance as seen from comparison with Figure 61a (theoretical accelerance) and 1/3 octave representation in Figure 61b. However, small errors exist in the vicinity of resonance. The H_2 estimator gives a poor accelerance in the vicinity of antiresonance as shown in Figures 62a-b (between 60 to 100Hz), while the H_4 estimator combines the advantages of both H_1 and H_2 as shown in the Figures 63a-b. This estimator however leads to some error in the vicinity of antiresonance compared to H_1 (compare Figures 61 and 63). Similar conditions occur with H_v although the errors are found to be greater than for H_4 (Figure

64). The H_s estimator seems to give results that are closest to H_I but leads to some errors in the multi-modal frequency range of 200 to 400Hz (compare Figures 61c and 65b).

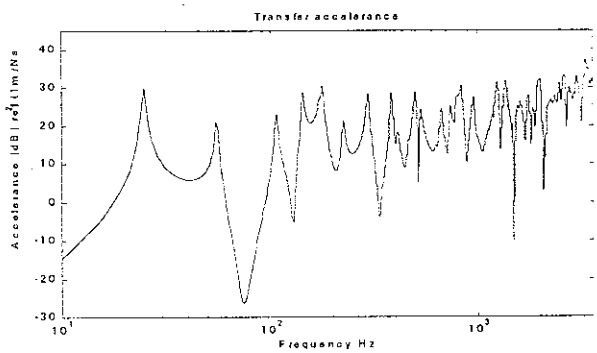

Figure 61a. Theoretical transfer accelerance from source location 1 to response location 1.

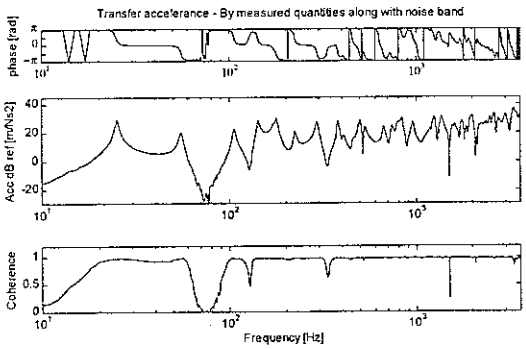

Figure 61b. Transfer accelerance by H_1 estimator from source location 1 to response location 1.

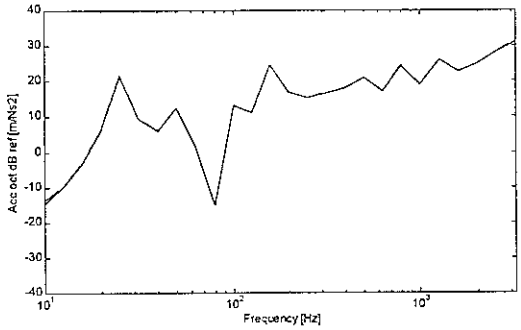

Figure 61c. 1/3 octave band transfer accelerance by H_1 estimator from source location 1 to response location 1. - - - ideal, _____ actual.

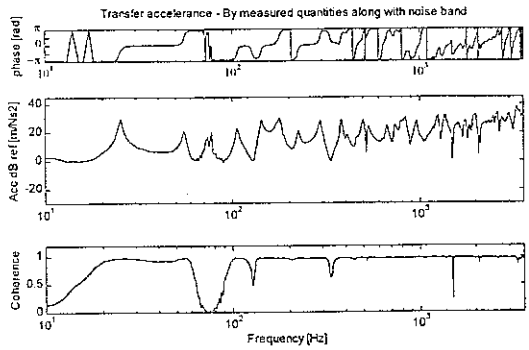

Figure 62a. Transfer accelerance by H_2 estimator from source location 1 to response location 1.

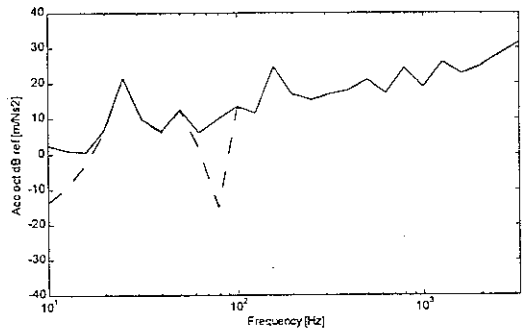

Figure 62b. 1/3 octave band transfer accelerance by H_2 estimator from source location 1 to response location 1. - - - ideal, _____ actual.

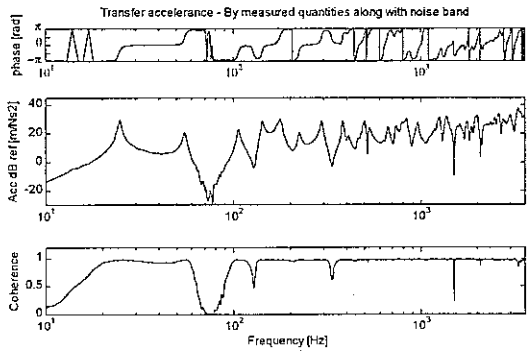

Figure 63a. Transfer accelerance by H_4 - Fabunmi estimator from source location 1 to response location 1.

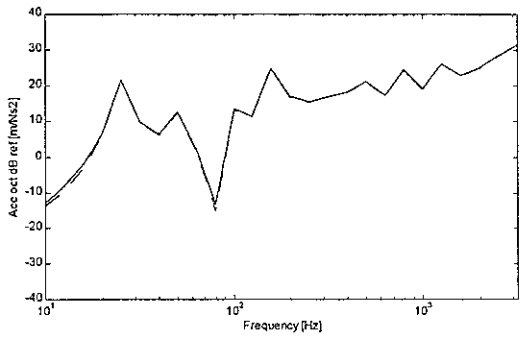

Figure 63b. 1/3 octave band transfer accelerance by H_4 - Fabunmi estimator from source location 1 to response location 1. - - - ideal, _____ actual.

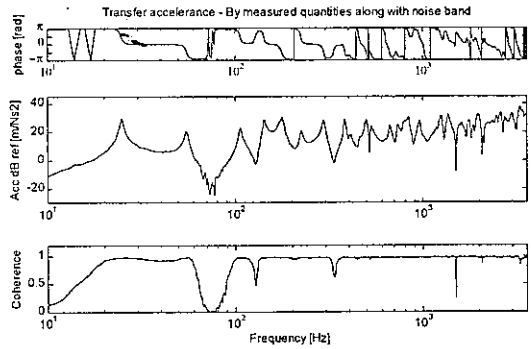

Figure 64a. Transfer accelerance by H_v estimator from source location 1 to response location 1.

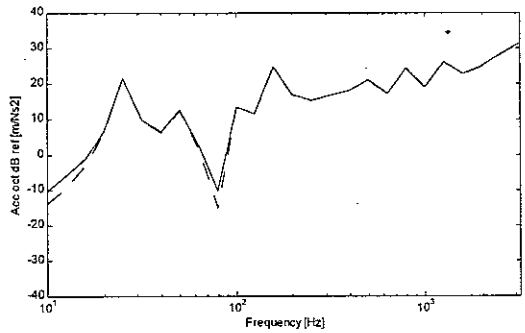

Figure 64b. 1/3 octave band transfer accelerance by H_v estimator from source location 1 to response location 1. - - - ideal, _____ actual.

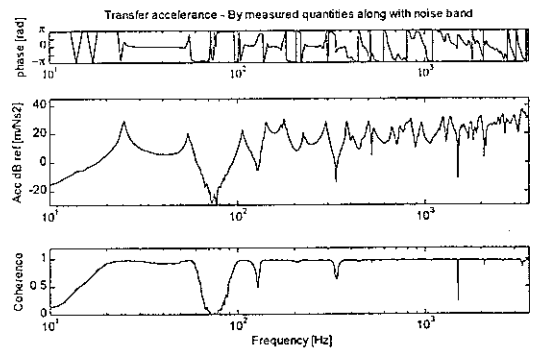

Figure 65a. Transfer accelerance by H_s estimator from source location 1 to response location 1.

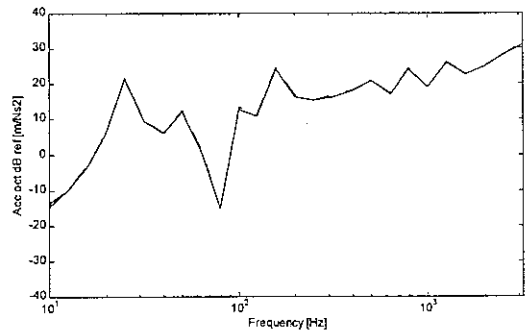

Figure 65b. 1/3 octave band transfer accelerance by H_s estimator from source location 1 to response location 1. - - - ideal, _____ actual.

These FRF estimators have been used in the construction of the accelerance matrix.

Following the procedure in [5], forces are reconstructed for each of the estimators.

6.2 Force reconstruction

Figures 66a-e show the force reconstruction for each of the estimators for 4 forces and 4 responses. Even though the H_1 estimator is biased near the resonance, it reconstructs the forces better than any other estimator considered. The H_2 estimator leads to the worst force reconstruction (Figure 66b). The results for the other estimators lie between those of H_1 and H_2.

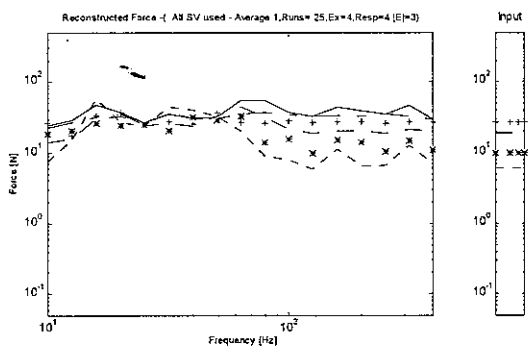

Figure 66a. 1/3 octave band reconstructed forces for 4 sources and 4 responses based on H_1 estimator with all singular values used.

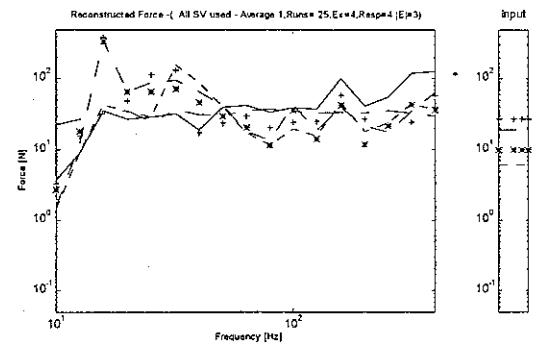

Figure 66b. 1/3 octave band reconstructed forces for 4 sources and 4 responses based on H_2 estimator with all singular values used.

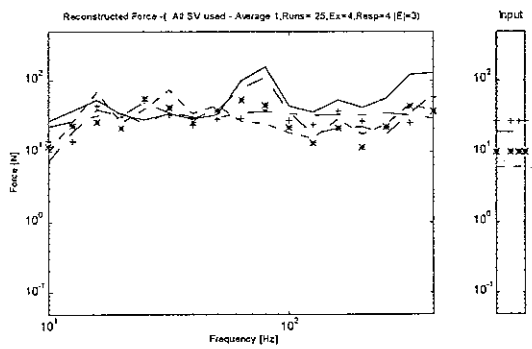

Figure 66c. 1/3 octave band reconstructed forces for 4 sources and 4 responses based on H_4 - Fabunmi estimator with all singular values used.

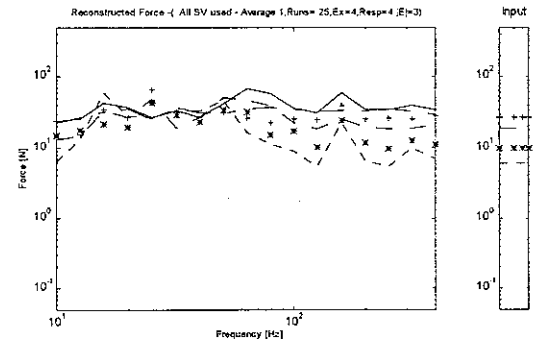

Figure 66d. 1/3 octave band reconstructed forces for 4 sources and 4 responses based on H_v estimator with all singular values used.

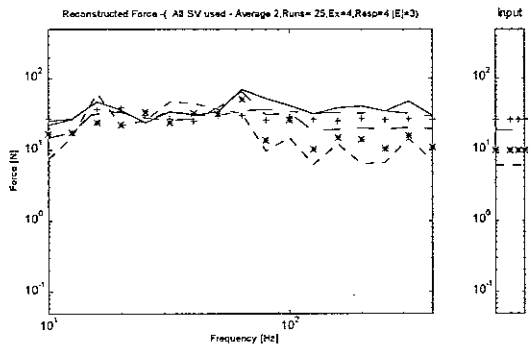

Figure 66e. 1/3 octave band reconstructed forces for 4 sources and 4 responses based on H_s estimator with all singular values used.

6.3 Velocity response at the receiver location

The velocity responses are shown in narrow band representation in Figures 67a-e for the various estimators. The predictions based on the H_1 estimator are better than those from any other estimator considered as seen from Figure 67a. The H_2 estimator leads to a spiky prediction at many of the frequencies (Figure 67b). Other estimators predict the responses with an accuracy which lies between the H_1 and H_2 based predictions.

Figures 68a-e show 1/3 octave representations of the velocity response at the receiver location. Again it is seen that the response based on the H_1 estimator is better than all the other estimators considered.

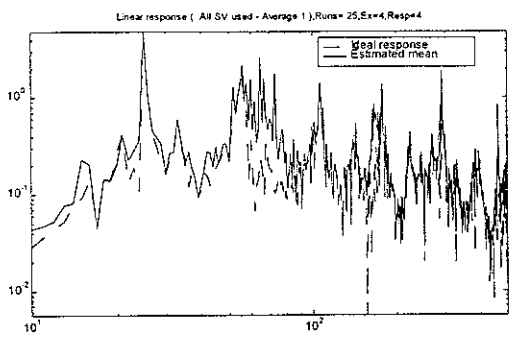

Figure 67a. Velocity response at the receiver location for 4 sources and 4 responses based on H_1 estimator with all singular values used.

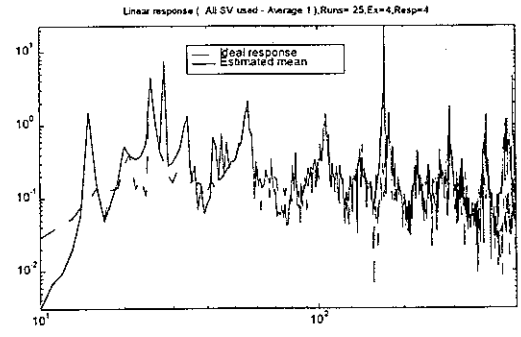

Figure 67b. Velocity response at the receiver location for 4 sources and 4 responses based on H_2 estimator with all singular values used.

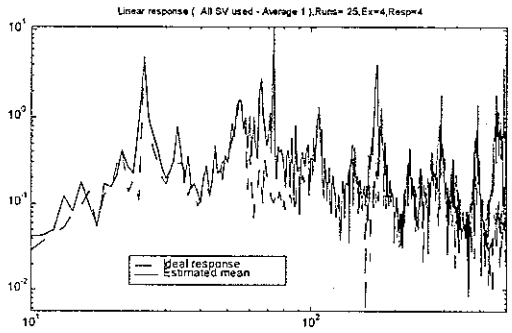

Figure 67c. Velocity response at the receiver location for 4 sources and 4 responses based on H_4 - Fabunmi estimator with all singular values used.

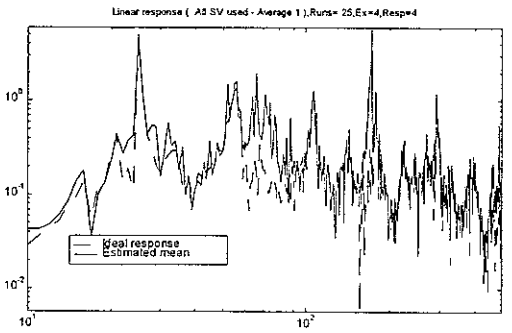

Figure 67a. Velocity response at the receiver location for 4 sources and 4 responses based on H_v estimator with all singular values used.

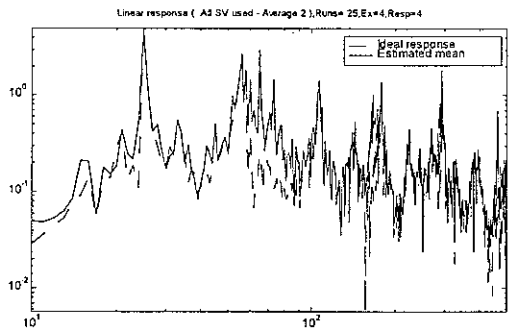

Figure 67e. Velocity response at the receiver location for 4 sources and 4 responses based on H_s estimator with all singular values used.

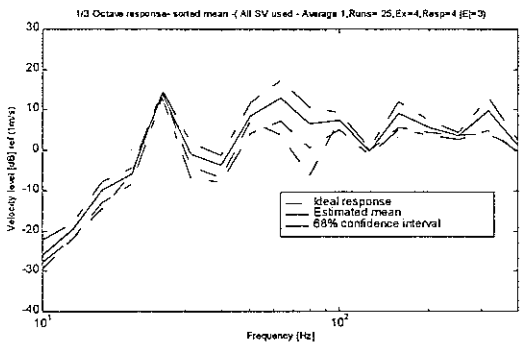

Figure 68a. 1/3 octave band velocity response at the receiver location for 4 sources and 4 responses based on H_1 estimator with all singular values used.

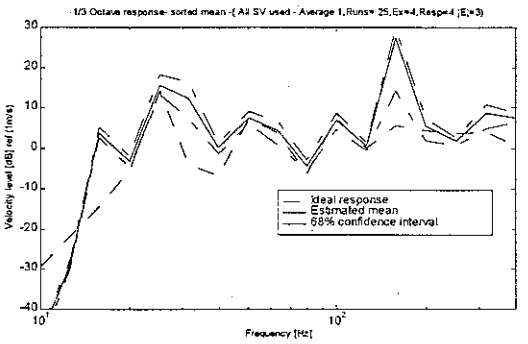

Figure 68b. 1/3 octave band velocity response at the receiver location for 4 sources and 4 responses based on H_2 estimator with all singular values used.

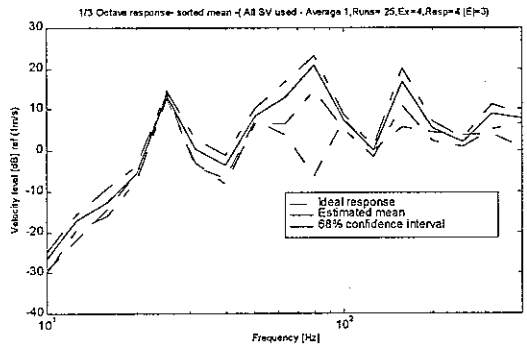

Figure 68c. 1/3 octave band velocity response at the receiver location for 4 sources and 4 responses based on H_4 - Fabunmi estimator with all singular values used.

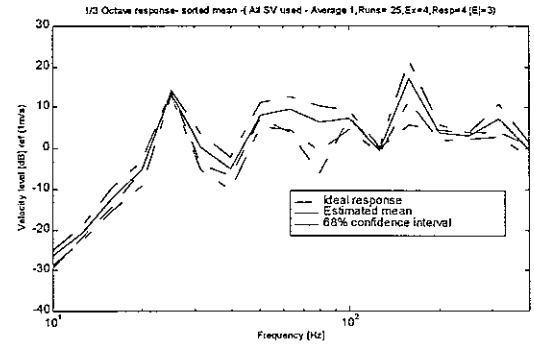

Figure 68d. 1/3 octave band velocity response at the receiver location for 4 sources and 4 responses based on H_v estimator with all singular values used.

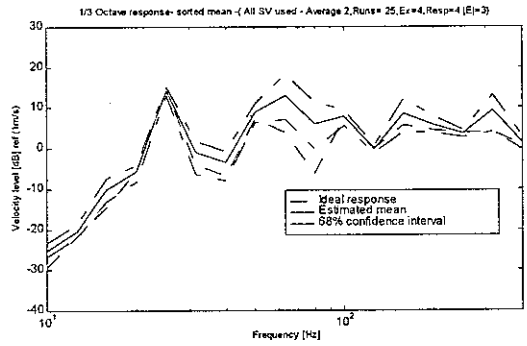

Figure 68e. 1/3 octave band velocity response at the receiver location for 4 sources and 4 responses based on H_s estimator with all singular values used.

6.4 Conclusions

The H_1 estimator, even it though has differing accuracy at resonance and antiresonance, results in a better force reconstruction across the frequency range in the inversion process than the other estimators considered. The H_s estimator gives results in the force reconstruction which are amost as good.

7. Error propagation

A complete understanding of error propagation plays a major role in devising ways to improve the force reconstruction. It is shown analytically and empirically by Blau [6] that random errors and bias errors propagate with different amplification during the process of force reconstruction. These error propagation models (as in [6]) are discussed below

7.1 Error propagation in force identification

It is well accepted [9] that the errors in the accelerance matrix and operational accelerations are magnified by at most the condition number 'κ' during the matrix inversion for force reconstruction. This can be written as

$$\left\|dS_{ff}\right\| \le \kappa^2 \left\|dA_{fa}\right\|$$

or (14)

$$\left\|dS_{ff}\right\| \le \kappa^2 \left\|dS_{aa}\right\|$$

where dS_{ff} - Error in the force spectral density estimation

dA_{fa} - Error in the accelerance estimation

dS_{aa} - Error in the operational acceleration spectral density estimation

NB : The condition number is squared since power spectral densities are used.

Quantitative error models are developed in [6] to characterise the contributions from various sources of errors in the process of force reconstruction by matrix inversion. These indicate that the magnification factors differ for various errors. The explanation given below follows ref [6]. Compared to the earlier studies by different researchers (eg. [10]), in [6] the estimations of error are made for individual forces each frequency rather than restricting consideration to the norm of vectors. This gives better insight into the whole

process. The reconstructed forces are characterised by their auto and cross spectral densities.

The propagation of the error is estimated based on the following formulation,

$$(S_{ff} + dS_{ff}) = (A_{fa} + dA_{fa})^{H+} (S_{aa} + dS_{aa})(A_{fa} + dA_{fa})^{+}$$

where f - force, a - response, and + is for pseudo-inversion.

Errors considered in [6] are, discussed below.

7.1.1. Errors on the response spectra

The spectral densities of response are calculated using finite fourier transforms of the measurements rather than continuous time histories. This results in variations from actual spectral densities. There are three aspects to this,

a. Time discretization - this never creates a problem as long as the sampling theorem is respected

b. Reduction of observation time to 'T' of finite length

c. Substitution of the expectation by averages.

'b' and 'c' yield a complicated error behaviour and errors due to these can be classified into two categories viz., random and bias errors.

Random errors :

Random errors describe the variation around the expected value. They are characterized by either the variance or the standard deviation. The standard deviation, when the response is represented as an auto spectral density, is inversely proportional to the square root of the number of averages [7]. This is based on the assumption that the random process is Gaussian. On the other hand, the standard deviation for cross spectral density is also related to the coherence function. Here the assumption is made that any random process contributing to the measured response signal occurs prior to the receiving

structure. Thus statistical characteristics of random errors on spectral density estimates will be the same whether estimates are made on the input side (force) or the output side (accelerations). Hence the error in force reconstruction due to this type of error can be taken to be proportional to the amplitude.

NB: Non-simultaneous acquisition of all the responses increases the random errors.

Measurement noise induced bias:

The measurement noise is used to refer to noise on the information channel from the sensor to the numerical representation of response spectra. It includes sensor noise, noise on cables, amplifier noise, quantization noise in analogue to digital conversion, round-off noise in spectrum calculation, etc. These all lead to the over-estimation of the response spectra and hence lead to the over-estimation of the force spectra. This error is amplified in proportion to the condition number of the accelerance matrix.

Leakage induced bias:

Leakage is the phenomenon appearing in the estimated spectra due to the convolution of actual spectra and the spectrum of the window used in signal processing. This leads to leakage of energy into the side bands. As leakage means virtually higher damping, the condition numbers decrease and hence leakage errors are more moderately amplified by the inversion process.

7.1.2 Errors on FRF's

Errors in frequency response function (FRF) measurement are also grouped into random and bias errors.

Random errors:

Using the ordinary coherence function, for random Gaussian additive noise, the variance in the estimation of FRF can be calculated as mentioned in [7].

In the force reconstruction, it is shown in [6] that the error amplication is bounded by terms containing both condition number and the square of the condition number. In contrast, in earlier theories the square of the error is multiplied only by the square of the condtion number.

Leakage induced bias:

Leakage induced bias errors are not magnified by the condition number during the inversion process. Errors are magnified moderately due to the reason discussed earlier for acceleration leakage error.

A summary of errors and error propagation models from [6] is shown in Table 1.

7.2 Current study

To confirm the above models and understand the propagation process, experiments are simulated to represent measurements which result in random and bias errors alone in the estimates. In this study, only the errors in the accelerance are considered while considering the operational accelerations as error free. The bias error is incorporated into the accelerance by introducing a measurement bias error in forces applied while estimating the accelerances. The accelerations are assumed error free. The random error is introduced by making the force measurement error free and incorporating random measurement noise into the accelerations. Figures 69 and 70 show the transfer accelerances from forcing loaction 1 to response loaction 1 for these errors. The accelerance matrices are formed for both cases and the forces are reconstructed using all singular values as in [5]. Figures 71a-b show the condition numbers of the accelerance matrix for both the cases. It is seen that the addition of random error alone reduces the condition numbers (compare Figures 71a and 71b).

Table 1. SUMMARY of error models [6]

Error type	Error charecteristic	Propagation to dS_{ff}	Distribution over dS_{ff}	Underlying assumption
Random errors on S_{aa}	As if force spectra were estimated directly			Response signals are acquired simultaneously , random errors of the estimates are not influenced by measurent noise
Measurement noise induced bias errors on S_{aa}	$S_{aa} + dS_{aa} = S_{aa} + S_{nn}$	$\varepsilon_{ff} \le \kappa^2(A_{fa})\varepsilon_{aa}$	$\lvert dS_{ffi,j}\rvert \approx \frac{\varepsilon_{ff}\lVert S_{ff}\rVert_F}{L}$	noise can be described by one uncorrelated zero mean random process per output
Leakage induced bias errors on S_{aa}	$S_{aa} + dSaa = D^H S_{aa} D$ $D = (1+a)I + E$ a - common relative error on all response spectral densities E - Matrix of complex random variables	$\varepsilon_{ff} \le 10Cs_{aa}$ Cs_{aa}=common relative error in S_{aa}	$\lvert dS_{ffi,j}\rvert \approx \frac{\varepsilon_{ff}\lVert S_{ff}\rVert_F}{L}$	Response signals are acquired simultaneously, transfer behaviour of the receiving structure can be described by a model with distinct resonances
Random errors on A_{fa}	$A_{fa} + dA_{fa} = A_{fa} + E$	$\left.\frac{\lvert dS_{ffij}\rvert}{\lVert S_{ff}\rVert_F}\right\rvert_{c2} \le \frac{\kappa^2(A_{fa})\varepsilon_{fa}^2}{L}$ $\left.\frac{\lvert dS_{ffii}\rvert}{S_{ffii}}\right\rvert_{c1,coh} \le \sqrt{\frac{\lVert S_{ff}\rVert_F}{S_{ffii}}}\kappa(A_{fa})\varepsilon_{fa}$		Shaker excitation, simultaneous acquisition of all responses, H_1 - estimate, no change of measurement setup between FRF and response measurements, noise/deviations from linearity can be described by one uncorrelated zero-mean noise process per output
Leakage induced bias errors on A_{fa}	$A_{fa} + dA_{fa} = D_1^H A_{fa} D_2$ $D_1 = (1+a_1)I + E_1$ $D_2 = (1+a_2)I + E_2$	$\varepsilon_{ff} \le 10CA_{fa}$ CA_{fy}=common relative error on A_{fa}	$\lvert dS_{ffi,j}\rvert \approx \frac{\varepsilon_{ff}\lVert S_{ff}\rVert_F}{L}$	As above (for random errors on FRFs), and transfer behaviour of the receiving structure can be described by a modal model with distinct resonances

Where L - number of forces, a_1 ,a_2- common relative errors on input and output side respectively (FRF)

E_1 ,E_2- Matrices of complex random variables

From matrix manipulation, the theoretical amplification of error is given by

$$\varepsilon(f) \le \kappa \frac{\left|\hat{error}(\hat{A})\right|}{\left|\hat{A}\right|} \tag{15}$$

where κ is a condition number of the accelerance matrix.

while the actual error amplification can be written as

$$\hat{\varepsilon}(f) = \frac{\left|\hat{F} - F\right|}{|F|} \tag{16}$$

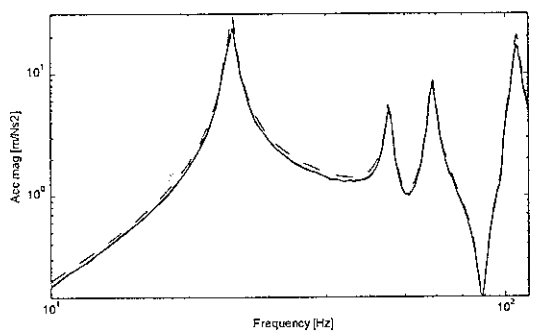

Figure 69a. Transfer accelerance from source location 1 to response location 1 for bias error alone in accelerance.

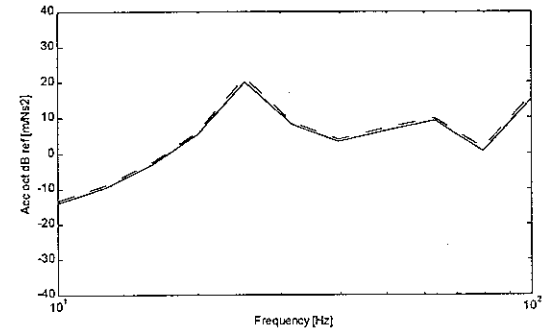

Figure 69b. Figure 70a. 1/3 octave band transfer accelerance from source location 1 to response location 1 for bias error alone in accelerance. - - - - ideal, _____ actual

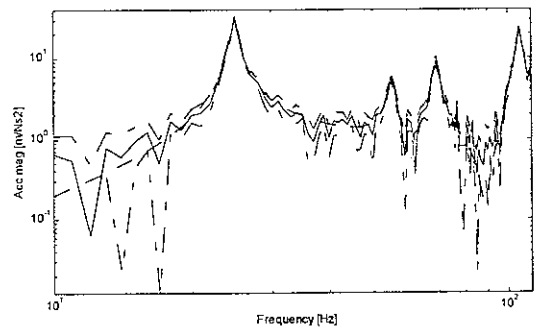

Figure 70a. Transfer accelerance from source location 1 to response location 1 for random error alone in accelerance.

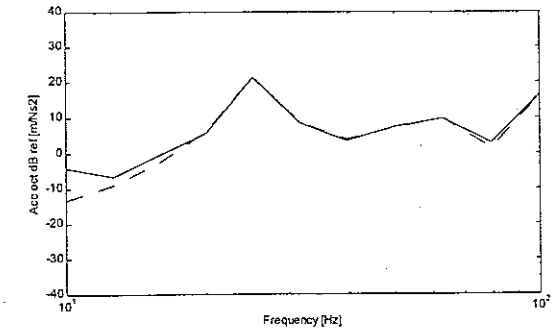

Figure 70b. 1/3 octave band transfer accelerance from source location 1 to response location 1 for random error alone in accelerance. - - - - ideal, _____ actual

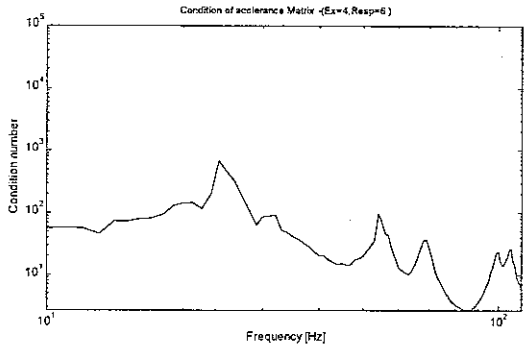

Figure 71a. Condition number of accelerance matrix at each frequency for bias error in accelerance.

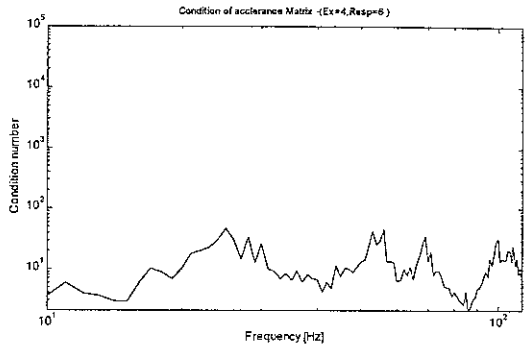

Figure 71b. Condition number of accelerance matrix at each frequency for random error in accelerance.

7.3 Force reconstruction

The force reconstruction with only bias error in the accelerance is shown in Figure 72a. The reconstruction is reliable except at the first resonance of the plate (26 Hz). In comparison with the bias error propagation, the random error results in worse force reconstruction (compare Figures 72b and 72a). This, however, may be due to larger random error in accelerances (compare Figures 69 and 70). If these errors are normalised (as in (15) and (16)) then it is possible to compare them.

The expected error magnification and the actual error magnification are shown in Figures 73-76. As seen from these figures, the magnification of error for bias error alone is less than the condition number at all frequencies for all forces (Figures 73a-76a). The relative error is observed to be high in the smallest of the forces reconstructed (Figure 76a - Force 4 is only 6 N). With random error alone the error magnification is by condition number or more than that (Figures 73b-76b). Again, the relative error in the smallest force is high (Figure 76b)

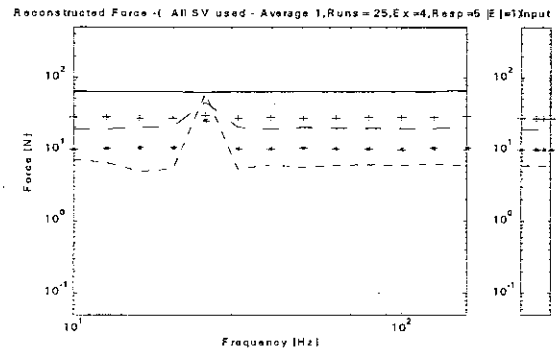

Figure 72a. 1/3 octave band reconstructed forces for 4 sources and 4 responses with all singular values used for bias error alone in accelerance.

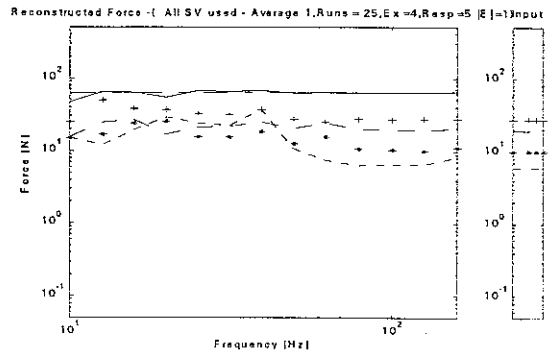

Figure 72b. 1/3 octave band reconstructed forces for 4 sources and 4 responses with all singular values used for random error alone in accelerance.

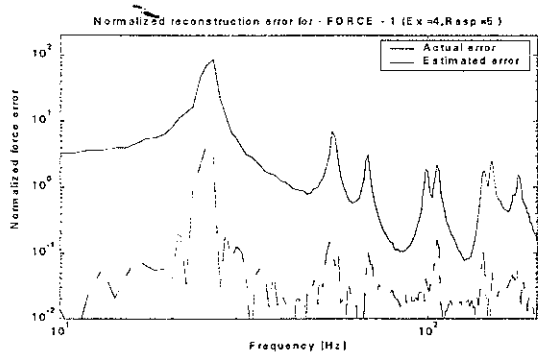

Figure 73a. Error in reconstructed force 1 for 4 sources and 4 responses with all singular values used for bias error alone in accelerance. _ _ _ Actual error, _____ Estimated error.

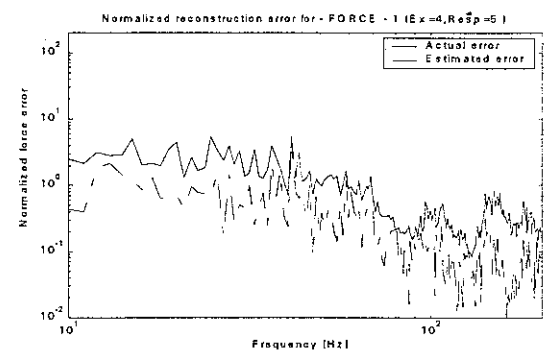

Figure 73b. Error in reconstructed force 1 for 4 sources and 4 responses with all singular values used for random error alone in accelerance. _ _ _ Actual error, _____ Estimated error.

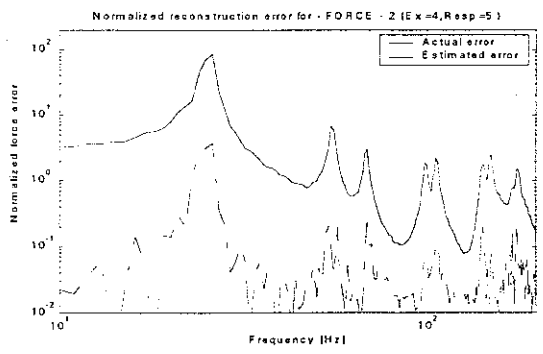

Figure 74a. Error in reconstructed force 2 for 4 sources and 4 responses with all singular values used for bias error alone in accelerance. _ _ _ Actual error, _____ Estimated error.

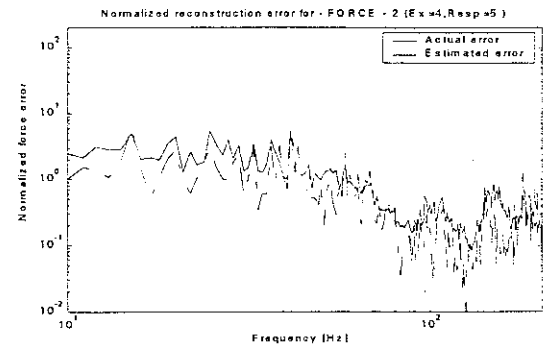

Figure 74b. Error in reconstructed force 2 for 4 sources and 4 responses with all singular values used for random error alone in accelerance. _ _ _ Actual error, _____ Estimated error.

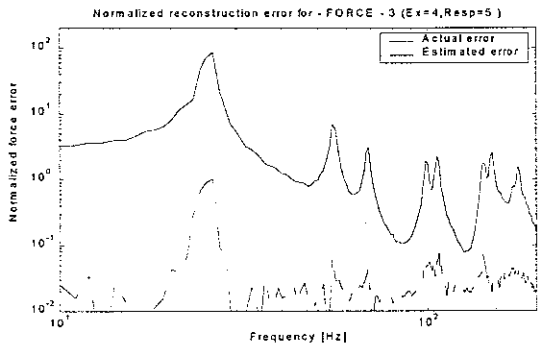

Figure 75a. Error in reconstructed force 3 for 4 sources and 4 responses with all singular values used for bias error alone in accelerance. __ _ __ Actual error, _____ Estimated error.

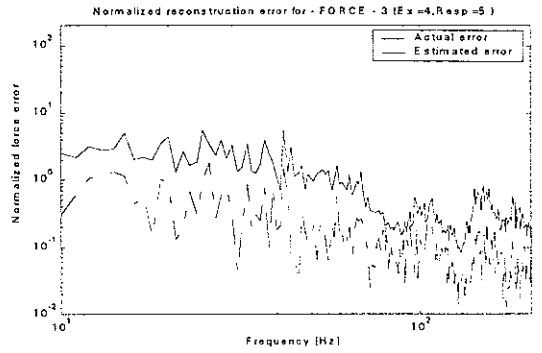

Figure 75b. Error in reconstructed force 3 for 4 sources and 4 responses with all singular values used for random error alone in accelerance. __ _ __ Actual error, _____ Estimated error.

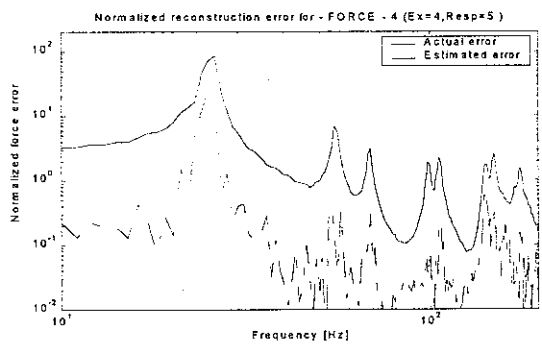

Figure 76a. Error in reconstructed force 4 for 4 sources and 4 responses with all singular values used for bias error alone in accelerance. __ _ __ Actual error, _____ Estimated error.

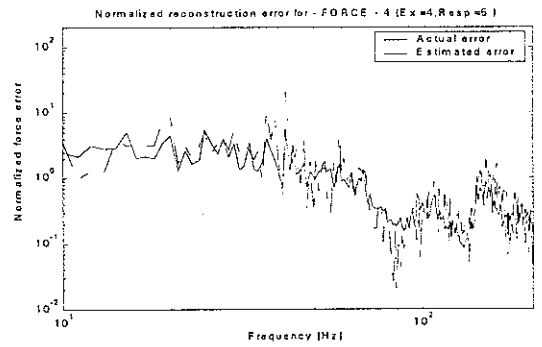

Figure 76b. Error in reconstructed force 4 for 4 sources and 4 responses with all singular values used for random error alone in accelerance. __ _ __ Actual error, _____ Estimated error.

7.4 Velocity response at the receiver location

Unlike the errors in the forces, the 1/3 octave velocity response at the receiver location does not differ much for the two types of errors (Figures 77a-b). At antiresonance, the random error alone results in a higher error. But the differences are large when narrow brand predictions are compared as shown in Figures 78a-b.

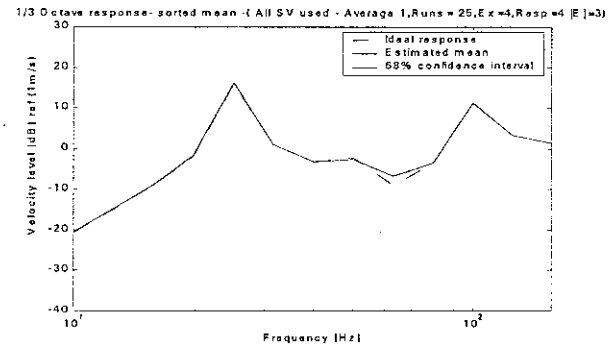

Figure 77a. 1/3 octave band velocity response for 4 sources and 4 responses with all singular values used for bias error alone in accelerance.

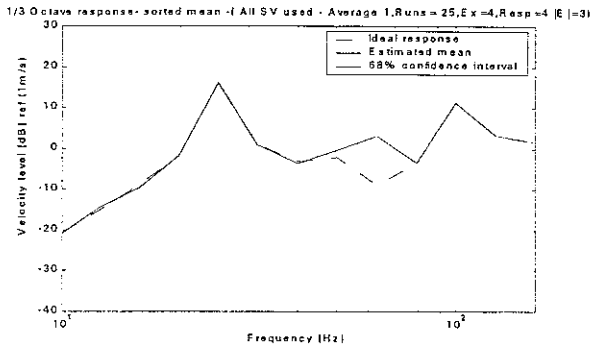

Figure 77b. 1/3 octave band velocity response for 4 sources and 4 responses with all singular values used for random error alone in accelerance.

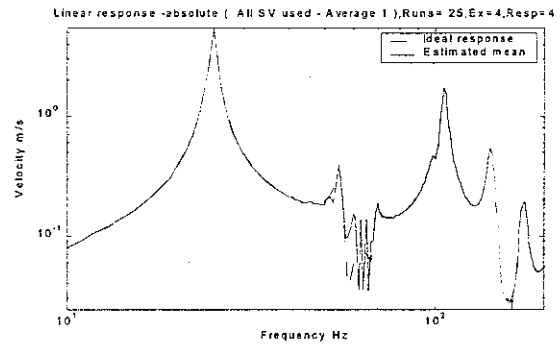

Figure 77a. Narrow band velocity response for 4 sources and 4 responses with all singular values used for bias error alone in accelerance.

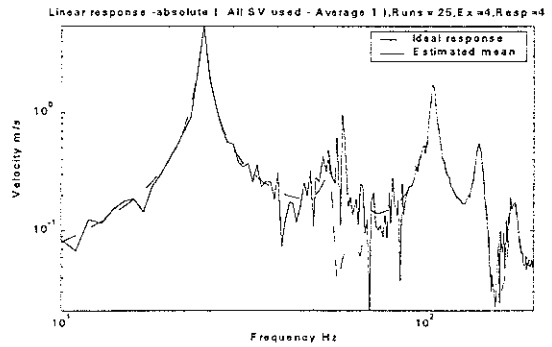

Figure 77b. Narrow band velocity response for 4 sources and 4 responses with all singular values used for random error alone in accelerance.

7.5 Conclusions

In general, a random error in the accelerance results in magnification in relation to the condition number or more in the force reconstruction process. The effect is largest on smaller forces. The bias errors however result in a magnification which is smaller than the condition number.

8. Conclusions

Using numerical simulations, force reconstruction and transfer path analysis has been carried out in continuation of the earlier work [5]. To investigate the sensitivity of earlier conclusions to phase information in the forces, forces with fixed phase at each frequency have been used. In the second study, rather high amplitude random noise has been used for corrupting the measured quantities. Further to this work, a proportional noise model with high noise amplitude has been implemented. The singular value rejection method to improve the force reconstruction has been further investigated for different threshold critaria. The sensitivity of force reconstruction to different FRF estimators and the error propagation have also been simulated to understand the errors in force reconstruction. The following conclusions are drawn based on these simulations.

1. The characteristics of force reconstruction and hence the 1/3 octave band response at the receiver location do not change whether or not the forces used have a non-zero relative phase.

2. The conclusions drawn in [5] differ slightly when considerably large corrupting noise is introduced to simulate the experimental 'measurements'. Under these circumstances, singular value rejection based on +/- one standard deviation band results in more reliable predictions than resampling (however, resampling predictions can be improved by taking a large number of averages which is seen to give better results even at antiresonance).

3. Use of a proportional Gaussian noise model does not alter the earlier conclusions [5]. In fact most of the strategies result in good predictions for this error model.

4. The predictions from singular value rejection, whether based on acceleration error or accelerance error, do not differ significantly from each other when the norm is based on +/- one standard deviation error band. In general the +/- one standard deviation band

results in better predictions than +/- 3 standard deviation. However, the improvements are not significant at frequencies where more than one mode contributes to the response and the condition number is high. This condition can arise at frequencies between two resonances and in the vicinity of antiresonance. At such frequencies, by discarding singular values the error in the estimation of forces would be less, but the response predictions seem to have higher errors.

5. When singular value rejection is based on estimates of the error in the operational accelerations, further improvements are acheived by resampling the accelerance matrix and considering the cumulative sum of singular values that are rejected. Also for the case of estimates of the accelerance error, good improvement is observed when the cumulative sum is taken for comparing with error norm. Hence, it is essential that singular values be rejected based on a comparison of the error norm with the cumulative sum of the smallest singular values.

6. The H_1 estimator, although is less accurate at resonance than at antiresonance, results in better force reconstruction across the frequency range in the inversion process than other FRF estimators considered. This might be explained by the conclusions in [6] that bias errors are magnified less strongly than random errors.

7. In general, random errors in the accelerance result in magnification by the condition number or more in the force reconstruction process. The effect is greater on the smaller forces. The bias errors, however, result in an error magnification which is smaller than the condition number.

9. References

1. M.H.A. Janssens, J.W. Verheij and D.J. Thompson 1999 Journal of Sound and Vibration 226, 305-328. The use of an equivalent forces method for the experimental quantification of structural sound transmission.

2. LMS application notes on transfer path analysis 1995. The qualification and quantification of vibro-acoustic transfer paths.

3. JW Verheij, Inverse and reciprocity methods for machinery noise source charectrization and sound path quantification, Part 1 : Sources. International Journal of Acoustics and Vibration, Vol 2, No1, 11-20 1997.

4. JW Verheij, Inverse and reciprocity methods for machinery noise source charectrization and sound path quantification, Part 2 : Transmission paths. International Journal of Acoustics and Vibration, Vol 2, No3, 103-112 1997.

5. AN Thite and DJ Thompson, Study of indirect force determination and transfer path analysis using numerical simulations for a flat plate. ISVR Technical memorandom no. 851, May 2000.

6. M Blau, Indirect measurement of multiple excitation spectra by FRF matrix inversion : Influence of errors in statistical estimates of FRFs and response - 1999 vol 85, 464-479 Acustica.

7. J.L. Bendat and A.G. Piersol 1993 Engineering application of correlation and spectral analysis. New York : Wiley interscience. 2nd edition.

8. MHA Janssens, JW Verheij and T Loyau, Experimental example of the pseudo-forces method used in characterisation of a structure-borne sound source. Paper submitted to Applied Acoustics.

9. GW Stewart, Introduction to Matrix Computations. Academic Press 1973.

10. TJ Roggenkamp and RJ Bernhard, Indirect measurement of multiple random force spectra - 1993, 881-884, Proceeding of Inter-noise.

11. CM Harris, Shock and Vibration Handbook, 4th Ed., Pub. McGraw-Hill, 1996.

12. JA Fabunmi and FA Tasker, Advanced Techniques for measuring structural mobilities. ASME Journal of Vibration, Acoustics, Stress and Reliability in Design, 345-349, Vol. 110, July 1988.

13. KS Hong and CB Yun, Improved method for frequency domain identification of structures. Engineering Structures, 1993 vol 15 No. 3, 179-188.

Appendix Different estimators of frequency response functions

H_1 estimator

This is a most popular estimator of the frequency response function and is based on the least square technique to reduce the effect of noise on the output. It is given by

$$H_1 = \frac{S_{xy}}{S_{xx}} \qquad \text{(A1)}$$

where $S_{xx} = \frac{1}{m}\sum_{i=1}^{m} X_i(f) * X_i(f)$ and $S_{xy} = \frac{1}{m}\sum_{i=1}^{m} X_i(f) * Y_i(f)$

and $X(f)$ and $Y(f)$ are Fourier transforms of x(t) and y(t) respectively and * indicates conjugation.

H_1 minimizes the effect of noise in the ouput. Provided the input is noise free, the H_1 estimator calculates an un-biased estimate of the frequency response function. At a resonance, as the input strength required for reasonable response is very low, the noise floor may affect the input measurement. This results in overestimation of the auto spectrum of x(t) as noise power also gets added to the signal. Hence, the FRF estimator H_1 is biased and less than the actual one at the resonances. Even at antiresonance H_1 is biased but the amount of bias is very small since the noise in the measured force is less.

Note : It is assumed that the noise in the input and output are not correlated and hence the cross spectrum is unbiased for a large number of averages.

H_2 estimator

This estimator is calculated based on a least square technique to reduce the effect of noise in the input. It is given by

$$H_2 = \frac{S_{yy}}{S_{xy}} \qquad \text{(A2)}$$

where $S_{yy} = \frac{1}{m}\sum_{i=1}^{m} Y_i(f) * Y_i(f)$

H_2 minimizes the effect of noise in the input. Provided the output is noise free, the H_2 estimator calculates an un-biased estimate of the frequency response function. At a resonance, as the response is very large, effect of the noise floor is minimal and hence the estimator approaches actual FRF. For the estimate to be unbiased the noise floor should be considerably lower than the response. This condition means that if the response is small enough to be corrupted by the noise floor, even at resonance, the estimate would be biased. At any frequency as the noise power gets added to the actual output, the auto spectrum of the output is overestimated. This over estimation depends on signal to noise ratio. The signal to noise ratio can be very low at antiresonance. Hence, at antiresonance the H_2 estimator would be biased and would be greater than the actual FRF. Even at resonance the H_2 is biased but the amount of bias is very small since the signal to noise ratio is large.

NB : H_1 always under-estimates the FRF, but at anti-resonance the bias error is low and the FRF approaches the actual one.

H_2 always over-estimates the FRF, but at resonance the bias error is low and FRF approaches the actual one.

H_v estimator

This estimator evaluates the FRF based on the minimization of the effect of noise on both input and output by a total least square method and is called an unbiased estimator [11]. The estimator is given by

$$H_v = \frac{S_{yy} - k_f S_{xx} + \sqrt{\left(k_f S_{xx} - S_{yy}\right)^2 + 4k_f S_{xy} S_{yx}}}{2S_{yx}} \qquad \text{(A3)}$$

where

$k_f = \frac{S_{nn}}{S_{mm}}$, is a ratio of input to output noise power.

When noise ratio tends to 0, the estimator approaches H_2 and if it tends to infinity it approaches H_1. In all other cases, where a significant amount of noise exists in both input and output, the estimator lies between H_2 and H_1. The major disadvantage with this estimator is that the ratio of noises has to be known before hand, which in general is difficult to estimate reliably.

H_4 - as given by Fabunmi (Total least square estimate)

It is also possible to obtain a total least square based estimator in terms of H_2 and H_1. The estimator [12] in this case is given as

$$H_4 = \frac{H_2\left[\frac{\gamma^2 F}{|H_1|^2} + 1\right]}{\frac{F}{|H_1|^2} + 1} \qquad \text{(A4)}$$

where

$$F = \frac{\int_{\omega_1}^{\omega_2} |S_{xy}|^2 d\omega}{\int_{\omega_1}^{\omega_2} |S_{xx}|^2 d\omega} \quad \text{and} \quad \text{coherence } \gamma^2 = \frac{|S_{xy}|^2}{S_{xx}.S_{yy}}$$

The weighting function F is formulated such that higher weight is given for H_2 at the resonances and for H_1 at antiresonances. Reasonably good results are obtained with a constant value of F over a large frequency range [12]. However further experiments indicated that this can give a good estimation either at resonance or antiresonance point. According to [12] rather than using a constant F, the weighting should be such that the ratio of F to H_1 approaches zero for resonance and infinity at antiresonance. The optimal value of F at each natural frequency is found to be inversely proportional to the imaginary part of H_2.

H_s estimator

If the signal to noise ratio is small, H_4 tends to have large errors at some frequencies. To overcome this difficulty in [13] it is suggested to use a different weighing function as given below

$$H_s = H_1(1-W) + H_2 W \tag{A5}$$

where

$$W = e^{\left(-\left(\frac{\frac{\omega_o}{\omega_n}-1}{\alpha}\right)^2\right)}$$

and

$$\omega_o = 0,1,.....2\omega_n$$

Here, the weighting is exponential and has a value 1 at resonance and reduces to zero exponentially at all other points. The exponential decay is inversely proportional to the damping factor [13], which in turn decides the magnitude of α. This estimator can give good results in the region of simple modal behaviour. Under multi-modal behaviour (high modal overlap), finding the weighting function at each frequency would be difficult.

The major assumption in the H_s and H_4 estimators is that, H_1 is unbiased at antiresonance and H_2 at resonance. In the majority of the cases where modal behaviour is predominant this assumption may be true. However, when the response at resonance is not so dominant or the force required at antiresonance is not high enough to be well clear of the noise floor, then this assumption would be violated and the estimator would still be biased.